Article

Cell Stem Cell

Long-Term Engraftment of Primary Bone Marrow Stromal Cells Repairs Niche Damage and Improves Hematopoietic Stem Cell Transplantation

Graphical Abstract

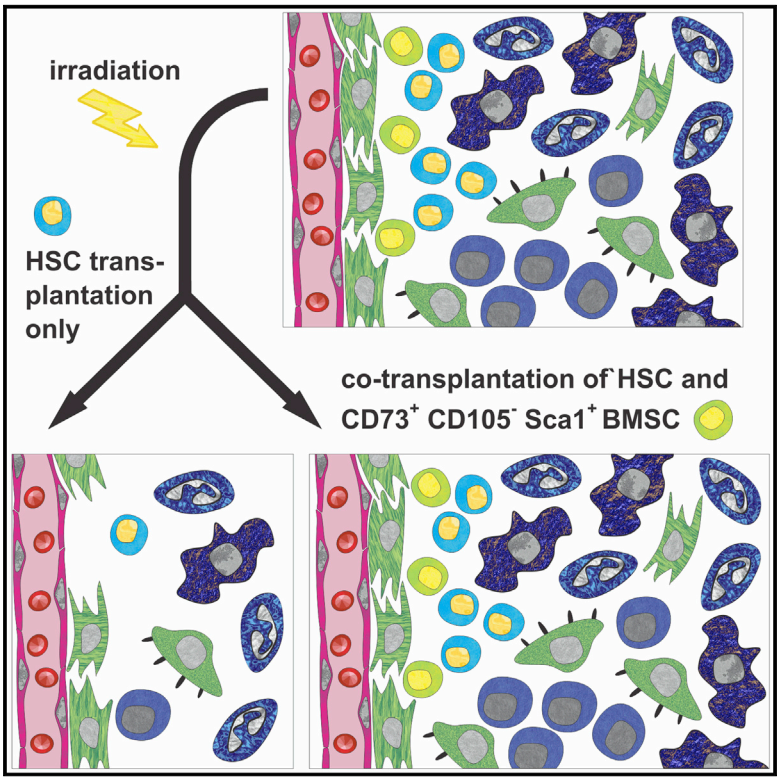

Authors

Jean-Paul Abbuehl, Zuzana Tatarova, Werner Held, Joerg Huelsken

Correspondence

joerg.huelsken@epfl.ch

In Brief

Abbuehl and colleagues show that irradiation required for hematopoietic stem cell (HSC) transplantation permanently damages the bone marrow (BM) stroma, which limits hematopoietic function. They develop protocols for intra-bone transplantation of multipotent BM stroma cells that reconstitute stroma function, thus significantly reducing clinically relevant side effects associated with HSC transplantation.

Highlights

- HSC transplant pre-conditioning irradiation permanently damages bone marrow stroma
- Loss of stroma function reduces HSC engraftment and number of functional HSCs
- Engrafted multipotent CD73^{+} CD105^{-} Sca1^{+} BM stromal cells localize to HSC niches
- Stromal repair boosts HSC numbers and rectifies granulopoiesis and B lymphopoiesis

Abbuehl et al., 2017, Cell Stem Cell *21*, 241–255
August 3, 2017
http://dx.doi.org/10.1016/j.stem.2017.07.004

CellPress

Cell Stem Cell
Article

Long-Term Engraftment of Primary Bone Marrow Stromal Cells Repairs Niche Damage and Improves Hematopoietic Stem Cell Transplantation

Jean-Paul Abbuehl,[1] Zuzana Tatarova,[1,2,3] Werner Held,[4] and Joerg Huelsken[1,5,*]
[1]École Polytechnique Fédérale de Lausanne (EPFL), ISREC (Swiss Institute for Experimental Cancer Research), Lausanne 1015, Switzerland
[2]Department of Biomedical Engineering, Knight Cancer Institute, Oregon Health and Science University, Portland, OR 97239, USA
[3]Department of Radiology, Brigham & Women's Hospital, Harvard Medical School, Boston, MA 02115, USA
[4]Ludwig Cancer Research Center, Department of Fundamental Oncology, University of Lausanne, 1066 Epalinges, Switzerland
[5]Lead Contact
*Correspondence: joerg.huelsken@epfl.ch
http://dx.doi.org/10.1016/j.stem.2017.07.004

SUMMARY

Hematopoietic stem cell (HSC) transplantation represents a curative treatment for various hematological disorders. However, delayed reconstitution of innate and adaptive immunity often causes fatal complications. HSC maintenance and lineage differentiation are supported by stromal niches, and we now find that bone marrow stroma cells (BMSCs) are severely and permanently damaged by the pre-conditioning irradiation required for efficient HSC transplantation. Using mouse models, we show that stromal insufficiency limits the number of donor-derived HSCs and B lymphopoiesis. Intra-bone transplantation of primary, but not cultured, BMSCs quantitatively reconstitutes stroma function in vivo, which is mediated by a multipotent NT5E^{+} (CD73)$^{+}$ ENG^{-} (CD105)$^{-}$ LY6A^{+} (SCA1)$^{+}$ BMSC subpopulation. BMSC co-transplantation doubles the number of functional, donor-derived HSCs and significantly reduces clinically relevant side effects associated with HSC transplantation including neutropenia and humoral immunodeficiency. These data demonstrate the potential of stroma recovery to improve HSC transplantation.

INTRODUCTION

Approximately 50,000 hematopoietic stem cell transplantations (HSC-T) are performed every year in order to treat patients with hematopoietic malignancy, aplastic anemia, and primary immunodeficiency (Majhail et al., 2012). Successful engraftment by exogenous HSCs requires a competitive advantage over endogenous HSCs, which is achieved by eliminating host marrow cells by combinations of chemotherapeutics and irradiation. The use of peripheral blood stem cells (PBSC), better prophylaxis against infection, refined immunosuppressive therapies to control graft-versus-host disease (GvHD), and reduced intensity conditioning (RIC) regimen with lower toxicities have improved overall survival over the last 2 decades (Majhail et al., 2012). Notwithstanding, HSC-T still entails significant risks for patients: the overall survival probability for adult leukemia patients who receive allo-HSCT is only about 50% (Anasetti et al., 2012), which increases to 85% for the following 10 years if patients survive the critical first 2 years (Wingard et al., 2011). About half of patient's deaths are due to leukemic relapse, while 15% are caused by either GvHD or infections. Post-transplant patients suffer from myelosuppression for several weeks and deteriorated adaptive immunity increasing the risk of opportunistic infections (Storek et al., 2008). Even in the absence of GvHD, most patients require about 1 year for adequate reconstitution of the adaptive immune system. Donor-derived adaptive immunity is typically poor, since post-transplant, homeostatic expansion of T cells restricts clonal diversity and limits T cell-dependent B cell responses (Norlin et al., 2008). Humoral immunity is further reduced due to insufficient B lymphopoiesis characterized by a lack of B cell precursors (Storek et al., 2008). B cell deficiency can be compensated by intravenous immunoglobulin replacement therapy, which, however, often produces side effects. Therefore, approaches increasing post-transplantation myelopoiesis and B lymphopoiesis may alleviate HSC-T related complications such as life-threatening infections.

Hematopoietic stem cells have the capacity to self-renew and to generate all differentiated cell types present in the blood. Among the cell populations present in the bone marrow (BM), HSCs are uniquely able to stably engraft the BM of a recipient and to expand and provide long-term multi-lineage hematopoiesis. A number of studies have demonstrated improved outcome of HSC-T with increased doses of CD34^{+} stem and progenitor cells indicating that their expansion capability may be limited (Pulsipher et al., 2009). In animal experiments, the number of donor HSCs after transplantation does not exceed around 10% of that present in controls even when excess amounts of HSCs are transplanted (Iscove and Nawa, 1997). This may explain the impaired hematopoiesis with respect to lineage progenitors in the BM in human patients, which is still observed several years post-HSC-T (Domenech et al., 1995). In the BM, HSCs are found in specialized stromal niches, which support HSC self-renewal and multipotency (Acar et al., 2015). However, sustained and quantitative engraftment by donor HSCs requires pre-conditioning using irradiation or chemotherapeutics (Tomita

et al., 1994), which ablates most of the hematopoietic system of the host. Without pre-conditioning, donor chimerism remains very low (Bhattacharya et al., 2009), indicating competition between donor and host HSCs for available niches. The niche supports HSCs by providing factors such as CXCL12 and Kit-ligand (or Stem Cell factor) and facilitates expansion without exhaustion. Given the proximity of dormant and cycling HSCs and committed progenitors within the BM, it is thought that the different hematopoietic populations are supported by distinct types of specialized niches (Ding and Morrison, 2013): e.g., arteriolar and sinusoidal niches that preferentially associate with either quiescent or proliferating HSCs, respectively (Itkin et al., 2016; Kunisaki et al., 2013). Understanding the biology of these niches may provide valuable therapeutic opportunities to improve hematopoiesis after transplantation or to correct hematopoietic disorders. For example, osteoblastic niches were shown to support B lymphopoiesis in the bone marrow (Wu et al., 2008).

Here, we find that pre-conditioning for HSC-T using total body irradiation (TBI) permanently incapacitates the BM stroma. This defect can be rescued by intra-bone transplantation of freshly isolated $CD73^+$ $CD105^-$ $SCA1^+$ multipotent bone marrow stromal stem cells but not using cultured cells. Indeed, the co-transplantation of HSCs with primary bone marrow stromal cells (BMSCs) markedly improves the expansion of donor-derived HSCs in irradiated hosts and reduces side effects of HSC-T such as neutropenia or B lymphocytopenia.

RESULTS

Irradiation Damages Stromal Niches in the Bone Marrow

Since irradiation damages DNA and thus targets proliferating cells, we used the colony-forming units fibroblasts (CFU-F) assay to estimate the content of proliferation-competent BM stromal cells after TBI at a dose (2 × 4.5 Gy, 4 hr apart) routinely used to pre-condition mice for HSC transplantation. Total bone marrow cells were isolated by first flushing the red marrow cavity (marrow suspension) and combining this preparation with cells isolated by crushing and treating the marrow-free bones with collagenase (endosteal and metaphysis fraction; Figure S1A). The latter preparation contained over 99% of CFU-F activity within the bone (Figure S1B). In contrast to controls, which gave rise to around 2,000 CFU-F per femur, irradiated mice showed an over 98% reduction of CFU-F activity 1 day after irradiation (Figure 1A). In order to determine whether TBI resulted in transient or permanent loss of CFU-F activity, we rescued hematopoiesis in irradiated mice by HSC-T (via systemic delivery by tail vein injection). Surprisingly, the CFU-F activity did not recover after 4 weeks and only marginally increased to 7% of controls after 4 months indicating that upon irradiation the stroma had permanently lost its ability to expand ex vivo. In agreement with these data, bone marrow stromal cells (BMSCs) isolated from irradiated, GFP^+ donors by magnetic activated cell sorting (MACS) to remove $CD45^+$, $CD11b^+$, LY76 $(Ter119)^+$, and $CD31^+$ (hematopoietic and endothelial lineage) cells (Figure S1C) did not engraft GFP^- recipients, while BMSCs from non-irradiated GFP^+ donors were readily detected 5 days after transplantation (Figure 1B). Further, stroma-derived factors and markers of stromal differentiation (*Kitl*, *Vcam1*, *Angpt1*, *Spp1*, *Adipoq*, *Sp7*) were severely reduced in BMSCs isolated 4 weeks after irradiation (and HSC-T) as compared to controls (Figure 1C). Together this indicates that the pre-conditioning, which is typically used for HSC engraftment leads to a severe and long-term defect of the BM stroma.

Importantly, the reduction in CFU-F activity is paralleled by a reduction of HSC numbers after transplantation. Transplanting 5 × 10E6 bone marrow cells (containing ~300 HSCs) into an irradiated mouse (which equals 2.5 × 10E8 BM cells per kilogram body weight and corresponds to the dose typically used in patients: 2–11 × 10E8 BM cells per kilogram body weight with about 1% of $CD34^+$ hematopoietic stem and progenitor cells; Sezer et al., 2000) failed to restore the number of HSCs present in non-irradiated control mice. While one femur of an irradiated recipient contained around 1,200 donor-derived HSCs (Lin^- $SCA1^+$ KIT^+ [LSK] $CD150^+$ $CD48^-$) after 4 weeks and 1,500 donor-derived HSCs after 12 weeks, around 8,400 HSCs were present in the femur of non-irradiated, non-transplanted control mice (Figures 1D and S1D). Together, these data reveal that pre-conditioning by irradiation permanently damages the BM stroma, which shows only insufficient, spontaneous recovery. The residual stroma may be ineffective at supporting HSC reconstitution.

We next addressed whether HSC engraftment could be improved by restoring the BM stroma. To test whether stromal cells were recruited to irradiation-damaged stromal niches in the bone via the circulation, we irradiated a single femur while protecting the remainder of the body with a lead mask. As expected, the exposed femur lost over 95% of its stromal progenitors within 5 days after irradiation. Interestingly, CFU-F activity only recovered to about 20% of the control levels after 4 weeks (Figure 1E). This suggested inefficient mobilization and recruitment of stromal cells via the circulation.

We thus performed rescue experiments with BMSCs by direct intra-bone transplantation instead of systemic delivery. Using cells obtained from BMSCs cultures (cBMSCs) expanded in vitro for 2 weeks did not improve the abundance of HSCs (Figure 1D). Together, these data reveal that pre-conditioning by irradiation permanently damages the BM stroma, which shows only insufficient, spontaneous recovery. The residual stroma may be ineffective at supporting HSC reconstitution.

Co-transplantation of Primary BMSCs Improves HSC Engraftment

We next tested whether the co-transplantation of primary BMSCs into both femurs enhanced the efficiency of HSC-T (Figure 2A). To track transplanted cells, we used HSCs from mice ubiquitously expressing GFP (ACTIN-GFP). However, since GFP triggered cell rejection in wild-type hosts (Figures S2A and S2B), we used recipient mice expressing GFP in the pancreas under the control of the rat insulin promoter, which did not reject GFP-expressing cells (Figure S2C). Intra-bone engraftment of primary BMSCs was further improved using Rho-associated protein kinase (ROCK) inhibitor Y-27632 (Figure S2D), which possibly prevents anoikis of cells (Watanabe et al., 2007). The co-transplantation of primary BMSCs had a significant effect on the abundance of Lin^- $SCA1^+$ KIT^+ (LSK) cells (Figure 2B) and increased the frequency and absolute number of HSCs (LSK $CD48^-$ $CD150^+$) and of LT-HSCs (LSK

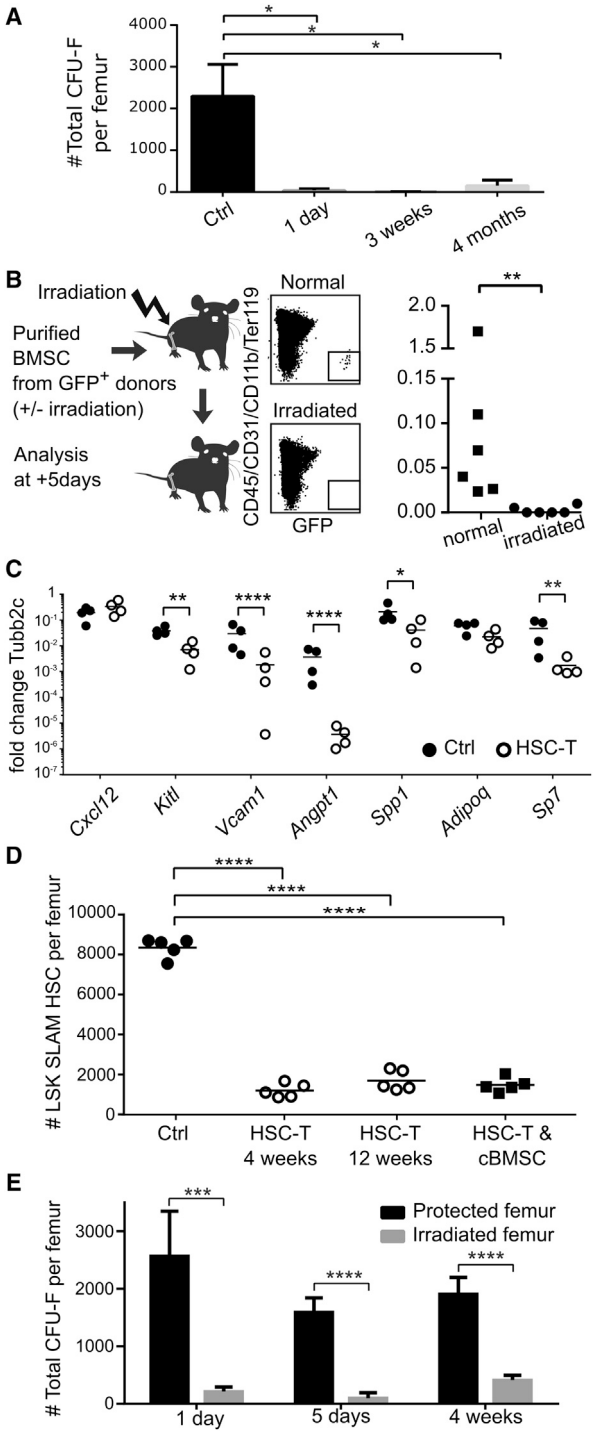

Figure 1. Stromal Niches in the BM Are Damaged by Irradiation

(A) Total colonies in CFU-F assays per femur after TBI (2 × 4.5 Gy) and HSC-T (except for day 1) as measured 1 day, 3 weeks, or 4 months after irradiation (n = 4 each; one-way ANOVA; error bars show SD; age-matched FVB animals were used as controls).

(B) Engraftment of MACS-enriched BM stromal cells extracted from either untreated control or irradiated GFP$^+$ donors was intra-femorally transplanted into irradiated GFP$^-$ hosts. Frequency of Lin$^-$ GFP$^+$ stromal cells as analyzed by flow cytometry after 5 days (n = 6, data pooled from two independent experiments; Mann-Whitney test).

(C) RT-qPCR for niche and lineage differentiation factors expressed in stromal cells from untreated controls and mice 4 weeks post-irradiation/transplantation (data pooled from four independent experiments; unpaired parametric t test). Stromal cells were directly isolated from the endosteal and metaphysis fraction of the femur by MACS-depletion of hematopoietic and endothelial lineages. *Spp1* codes for OSTEOPONTIN and *Sp7* codes for OSTERIX (n = 4, unpaired parametric t test).

(D) Quantification of HSCs (Lin$^-$ SCA1$^+$ KIT$^+$ CD150$^+$ CD48$^-$) per femur in age-matched controls, chimeric mice (4 and 12 weeks after TBI and HSC-T), and chimeric mice co-transplanted with 50,000 BM stromal cells isolated by 2 weeks of in vitro expansion (4 weeks after TBI and transplantations; n = 5 each; unpaired parametric t test).

(E) Total colonies in CFU-F assays per femur after local irradiation (2 × 4.5 Gy) of one femur in comparison to the contralateral, non-irradiated femur (rest of the body protected by a lead mask) as measured 1 day, 5 days, and 4 weeks after irradiation (n = 4 each, paired parametric t test; error bars show SD).

See also Figure S1.

CD48$^-$ CD150$^+$ CD34$^-$) 4 weeks post-transplantation (Figures 2C and 2D). Competitive, long-term (16 weeks) reconstitution assays in secondary recipients confirmed expansion of functional HSCs in hosts co-transplanted with primary BMSCs and HSCs as compared to classical HSC-T alone (Figures 2E, 2F, and S2E–S2G). Chimerism at 16 weeks was more than doubled, and donor-derived contribution to the granulocytic (Gr1$^+$ CD3$^-$ B220$^-$) lineage increased over 3-fold by co-transplantation with primary BMSCs and HSCs.

In contrast to primary BMSCs, HSC abundance remained low when the co-transplanted cells were obtained from BMSC cultures (cBMSCs) expanded in vitro for 2 weeks (Figure 2H; these data are displayed as fold change in comparison to HSC-T alone). If anything, cBMSCs decreased HSC and LT-HSC numbers and promoted the differentiation of common lymphoid progenitors (CLPs), which is in line with a lymphoid bias in patients receiving cultured BMSCs together with HSC-T (Ball et al., 2007). This may be due to altered expression of key regulators of HSC maintenance in primary as compared to cultured BMSCs. Indeed, *Spp1* (OSTEOPONTIN), which limits the size of the HSC pool (Stier et al., 2005), is strongly upregulated (300-fold) upon in vitro culture. This may blunt the effect of enhanced *Kitl* expression (30-fold) in cBMSCs (Figure 2I; *Cxcl12* was not significantly altered, data not shown). Failure of the in-vitro-expanded cBMSCs to expand HSCs was confirmed by secondary reconstitution assays (Figures 2E, 2F, and S2E–S2G). Thus, only primary BMSCs significantly expanded the abundance of functional HSCs in irradiated recipients, indicating that deficient stromal support induced by TBI limited the number of HSCs.

The beneficial effects of BMSC transplantation could be due to local or systemic effects. Restricting co-transplantation to only one femur allowed a direct comparison of HSC numbers in contralateral bones. We first ensured that donor-derived (GFP$^+$) stromal cells transplanted into one femur were only very inefficiently recruited to the contralateral femur (Figure 3A). LT-HSCs were significantly more abundant in the primary BMSC-transplanted femur (Figure 3B). Interestingly, an increased number of HSCs and LT-HSCs was also observed when primary BMSCs were transplanted 4 weeks after the initial HSC-T (Figures 3C and 3D), indicating that HSCs dynamically responded to the presence of BMSCs and expanded as a function of available niche support. Competitive reconstitution assays in

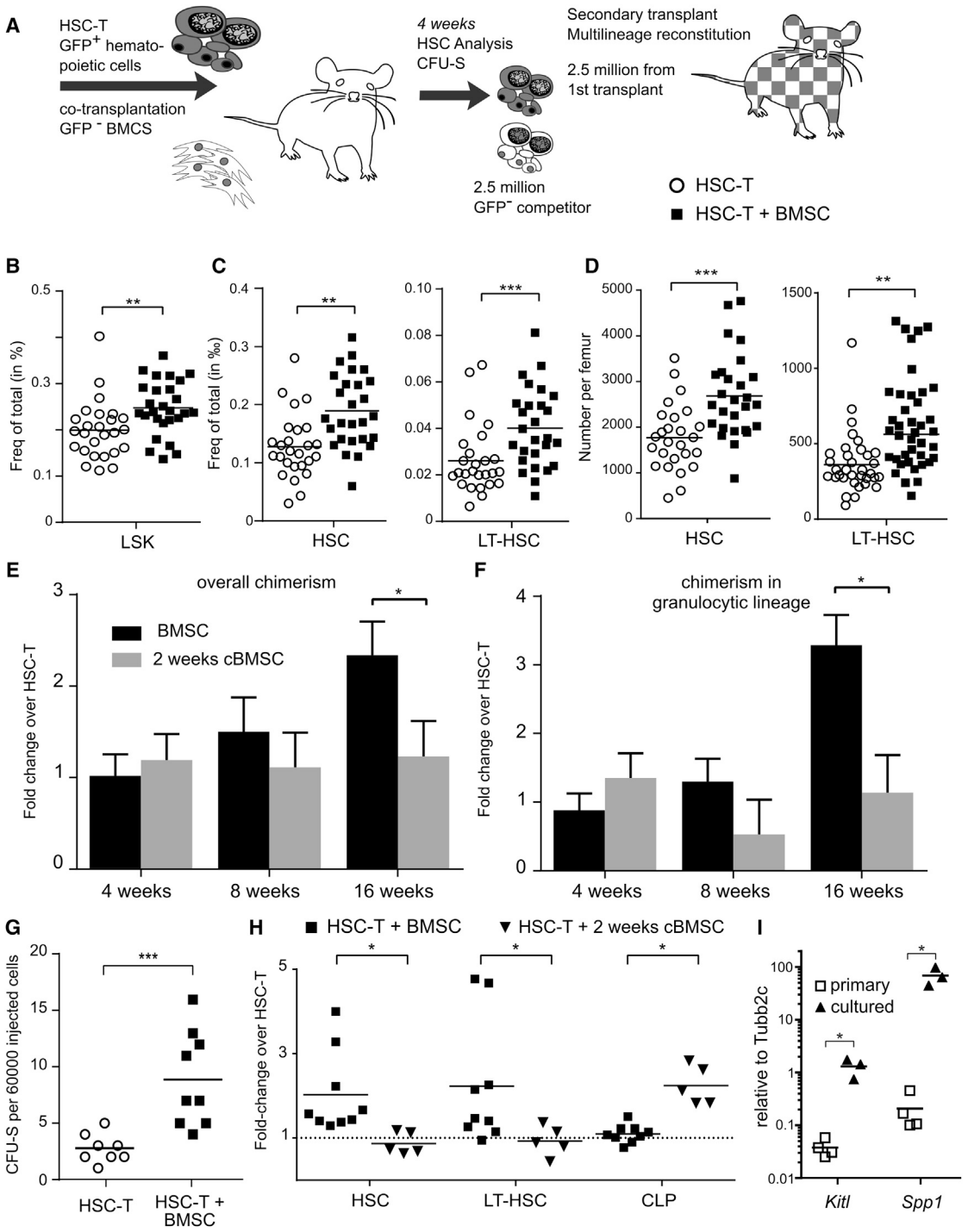

Figure 2. Reconstitution of HSCs Is Improved by BMSC Co-transplantation

(A) Schematic overview of the experiment: following TBI, mice were transplanted with GFP$^+$ BM containing HSCs with or without GFP$^-$ MACS-enriched BMSCs. After 4 weeks, 2.5 million GFP$^+$ hematopoietic cells were isolated, mixed with an equal amount of GFP$^-$ hematopoietic competitor cells, and transplanted into secondary hosts. The relative contribution of GFP$^+$ HSCs to hematopoietic lineages was analyzed 16 weeks later. The symbols listed apply to (B)–(E) and (G).

(B) Frequency of Lin$^-$ SCA1$^+$ c-kit$^+$ (LSK) was compared between recipients receiving standard HSC-T after TBI or co-transplantation of BMSCs (n = 26–27, pooled from five independent experiments; unpaired parametric t test).

(C and D) Frequency (C) or absolute numbers of HSCs (measured as Lin$^-$ SCA1$^+$ c-kit$^+$ CD150$^+$ CD48$^-$) and long-term HSCs (LT-HSC; measured as Lin$^-$ SCA1$^+$ c-kit$^+$ CD150$^+$ CD48$^-$ CD34$^-$) per femur (D) in recipients receiving TBI plus HSC-T with or without BMSCs (n = 26–27; unpaired parametric t test).

(E and F) Analysis of peripheral blood cells of secondary recipients transplanted with 1:1 mixtures of GFP$^-$ and GFP$^+$ hematopoietic cells (isolated from primary recipients after HSC-T with or without co-transplantation of primary BMSCs, or co-transplantation of 2 week in-vitro-cultured BM stroma [cBMSCs]). Flow

(legend continued on next page)

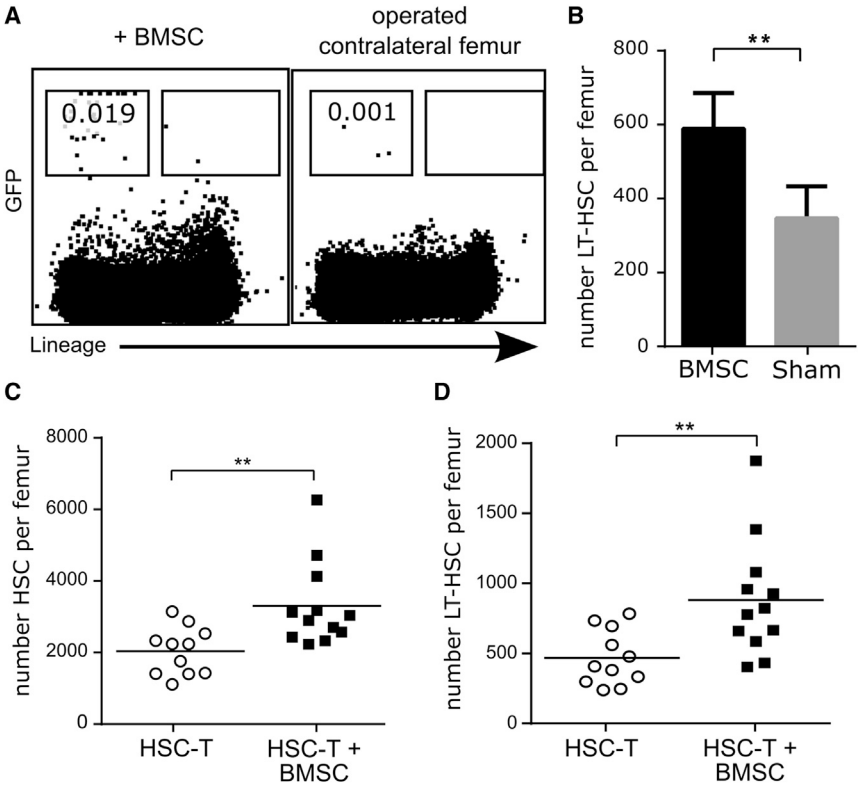

Figure 3. BMSC Transplantation Supports LT-HSC Expansion

(A and B) Flow cytometry to quantify GFP$^+$ BM stroma engraftment (A) and LT-HSC numbers per femur (B) 4 weeks after TBI/HSC-T and BMSC co-transplantation in only one femur comparing the co-transplanted with the contralateral, sham-operated femur (n = 4 each; paired parametric t test; error bars show SD).

(C and D) Numbers of HSCs (C) or LT-HSCs (D) per femur in in mice treated with TBI/HSC-T without or with 4 weeks delayed co-transplantation of BMSCs. Mice were analyzed 8 weeks after the initial TBI/HSCT (n = 11–12; data pooled from two independent experiments; unpaired parametric t test).

See also Figure S2.

secondary recipients confirmed the increased abundance of HSCs upon delayed BMSC transplantation; however, due to the limited sample size the data did not reach statistical significance (data not shown). We conclude that BMSCs have a limited ability to systemically support hematopoiesis or to be mobilized. Primary BMSCs can dynamically expand the abundance of HSCs, indicating that the size and/or quality of HSC niches can be restored and modulated even post-HSC-T by providing exogenous stromal cells.

Co-transplantation of BMSCs Reduces Clinically Relevant Side Effects of HSC-T

Post-transplantation patients suffer from neutropenia and weak adaptive immunity, which increases the risk of opportunistic infections and poses major clinical problems. We thus evaluated whether BMSC co-transplantation (GFP$^+$ cells into both femurs) as compared to classical HSC-T reduced some of these side effects. As expected, severe leukopenia (leukocyte levels less than 10% of controls) was observed in the peripheral blood 7 days after HSC-T (Figure 4A). After 14 days, recovery of leukocytes and in particular neutrophils as well as lymphocytes was improved at least 2-fold by co-transplantation of BMSCs (Figures 4A–4C; mice without successful engraftment of GFP$^+$ BMSCs were excluded [one of 14], i.e., those yielding <20 CFU-F, which is the baseline in HSC-T without BMSC co-transplantation). Thrombocytopenia or anemia is not observed upon HSC-T in mice and was not affected by co-transplantation (data not shown). Mature B cells were decreased 3-fold 4 weeks after HSC-T compared to non-irradiated and non-transplanted controls. Co-transplantation of BMSCs slightly increased mature B cells; however, this was not statistically significant ($p < 0.07$) (Figure 4D). Several early B cell developmental stages, including proB cells and fraction B and C' of preB cell development, were significantly increased when BMSCs were combined with HSC-T (Figures 4E–4J and S3A). Inefficient B lymphopoiesis in mice transplanted only with HSCs may be due to stromal damage and reduced production of stroma-derived factors known to support B cell development such as interleukin-6 (IL-6), IL-7, or insulin growth factor (IGF)-1 (Figure 4K; Yu et al., 2016). Consistent with improved B lymphopoises, splenic transitional B cells were significantly increased by BMSC co-transplantation (Figures 4L and S3B–S3G). Functionally, BMSC co-transplantation resulted in increased antigen-specific immunoglobulin M (IgM) production in response to immunization with the T cell-independent hapten tri-nitrophenyl (TNP; Figure 4M). These data

cytometry was performed at 4, 8, and 16 weeks to measure the fold change of overall chimerism (E) and the fold change within the granulocytic lineage (F) (Gr1$^+$ B220$^-$ CD3$^-$) when comparing HSC-T without BMSCs or HSC-T with BMSC co-transplantation (n = 14 for HSC-T and HSCT-T with BMSCs, n = 5 for HSC-T and HSC-T with cBMSCs; unpaired parametric t test; error bars show SD).

(G) Colony-forming units spleen (CFU-S) measured 12 days after secondary transplantation of BM isolated from primary recipients treated with TBI/HSC-T with or without co-transplantation with BMSCs (n = 9 each; unpaired parametric t test).

(H) Fold change in the frequency of HSCs, LT- HSCs, and CLPs upon co-transplantation with either primary BMSCs or cBMSCs. The results are shown relative to controls, which were performed with the identical BM preparations but without co-transplanted stroma (n = 9 for primary and n = 5 for cBMSCs; t test and correction for multiple comparisons).

(I) RT-qPCR for *Kitl* and *Spp1* expression in primary BMSCs or cBMSCs (n = 3–4; unpaired parametric t test).

See also Figure S2.

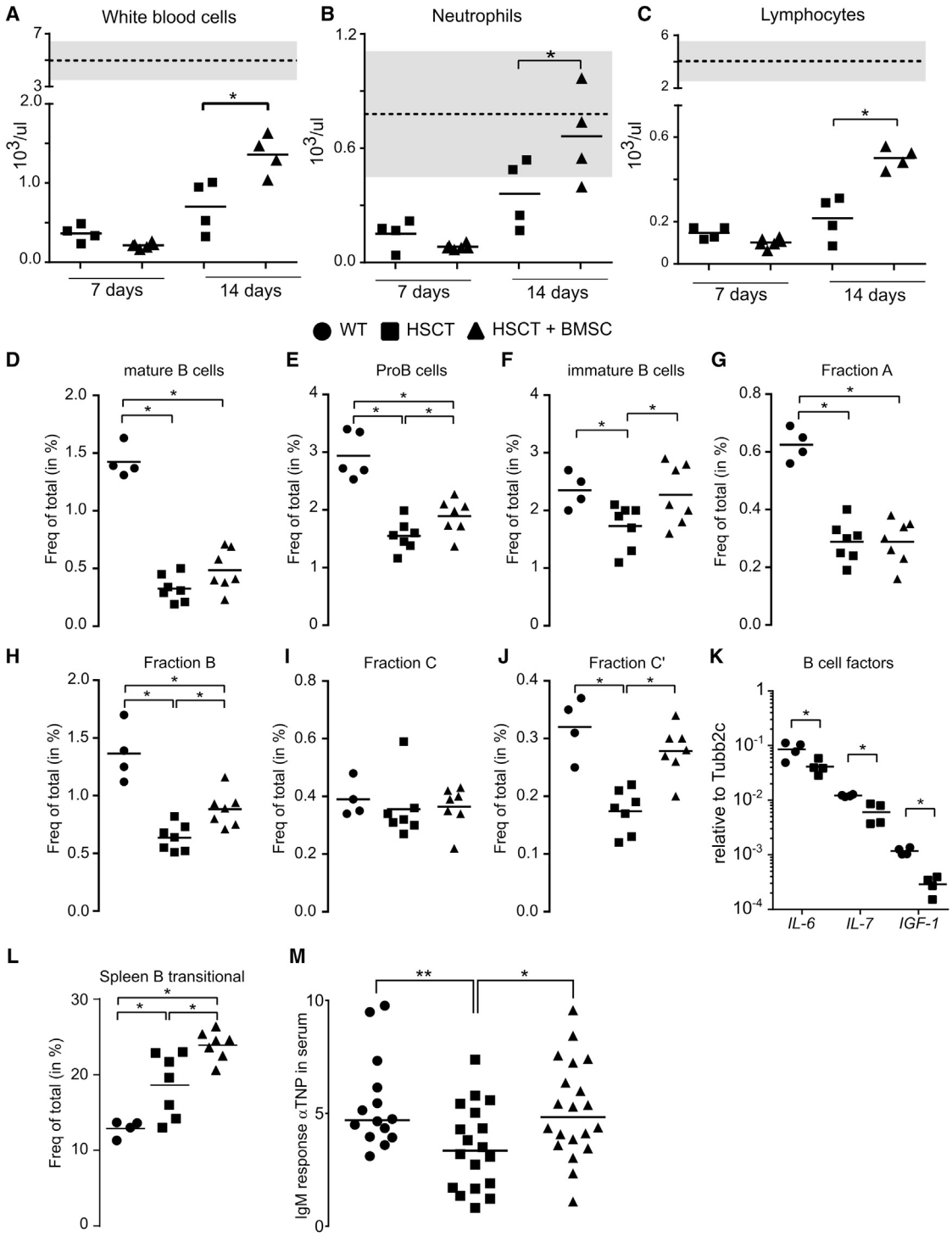

Figure 4. Accelerated Recovery of Clinical Parameters and B Lymphopoiesis by BMSC Co-transplantation

(A–C) White blood cell (A), neutrophil (B), and lymphocyte (C) counts in peripheral blood 7 and 14 days after TBI/HSC-T (2.5×10^6 BM cells) with or without BMSC co-transplantation (5×10^4). Diagrams show mean value (±SD, n = 4) as compared to controls prior TBI/HSC-T (depicted as broken line [mean] and gray box [SD])). The analyses include only mice with successful BMSC engraftment (four of five) (i.e., >20 donor-derived CFU-F at time of sacrifice, which is above the baseline after TBI) (data are from one experiment and representative of two independent experiments; unpaired one-way ANOVA non parametric, Turkey correction for multiple comparisons). The symbols for the different experimental mice apply to all figures.

(D–J) Quantification of BM B lymphopoiesis of untreated, age-matched wild-type mice and after TBI/HSC-T without or with BMSC co-transplantation (plots are representative, n = 4 or 7 mice per group in two independent experiments; unpaired parametric t test). (D) $CD3^-CD8a^-Gr1^-IgM^+B220^{high}$ mature B cells, (E) $CD3^-CD8a^-Gr1^-IgM^-B220^{high}$ ProB cells (F) $CD3^-CD8a^-Gr1^-IgM^+B220^{int}$ immature B cells, (G) $CD3^-CD8a^-Gr1^-IgM\text{-}B220^{int}CD43^{int}CD24^-BP1^-$ Fraction A,

(legend continued on next page)

indicate that new strategies, which improve stromal recovery or limit stromal damage, may provide clinical benefit to HSC-T patients.

Phenotype of Engrafting BMSCs

We next used known surface markers of mesenchymal stroma cells (CD73, CD105, SCA1, CD140a, CD44), to define the engrafting BMSC population. Five days after irradiation and BMSC transplantation, engrafted cells were predominantly $CD73^{hi}$ $SCA1^{hi}$ $CD140a^{+}$ cells, while CD44 was intermediate, and CD105 expression was absent (Figures 5A and 5B). The $CD73^{+}$ $CD105^{-}$ $SCA1^{+}$ population is rare (around 3%) in BMSCs (Figures 5C and S4B). When the analysis was performed 9 weeks after irradiation, the transplanted cells were still all $CD73^{+}$ and CD140a intermediate; however, CD105 expression was increased, and SCA1 expression was strongly decreased (Figure 5D). This indicates an initial selection for a rare, engrafting BMSC sub-population upon transplantation, followed by the re-generation of phenotypes present in the initial BMSC population.

We used the CFU-F assay to determine the number of clonogenic cells in different BMSC sub-populations. CFU-F activity was confined to the $CD73^{+}$ population (Figure 5E), which accounts for around 60% of all BMSCs (Figure 5A). Further, CFU-F activity was enriched in the $CD105^{-}$, the $CD44^{-}$, and the $SCA1^{+}$ populations. The marker CD140a (PDGFR) did not correlate with CFU-F activity. By extending this analysis to marker combinations within the $CD73^{+}$ subpopulation (Figure 5F), the highest CFU-F activity was found among $CD73^{+}$ $CD105^{-}$ cells, which was in perfect agreement with the phenotype selected in vivo (Figure 5A).

Since numerous studies of BM stromal cells are based on in-vitro-expanded cells, we evaluated the expression of the above markers after 2 weeks of in vitro culture starting from purified BMSC subpopulations (Figure S4A). The expression or the absence of CD73 remained stable. Similarly, expression of CD105 was hardly altered upon in vitro culture and only minor fractions (10%–20%) of CD105-defined cells changed their phenotype. In contrast, CD44, CD140a, and SCA1 expression was dynamic whereby negative cells gained marker expression in vitro while the majority of $CD140a^{+}$ cells lost this marker during culture (Figure S4A). Strikingly, the $CD73^{+}$ $CD105^{-}$ $SCA1^{+}$ population, which had the capacity to engraft, was lost upon in vitro expansion (Figure S4B). These findings highlight significant phenotypic changes of BMSCs during in vitro culture, which may explain why these cultured cells fail to support HSC function following irradiation and transplantation.

The beneficial effects of BMSC transplantation could be due to transient modulation of the BM microenvironment or to a long-term engraftment of progenitor cells, which reconstitute stromal niches in the BM. We therefore analyzed the long-term maintenance and fate of transplanted BMSCs in vivo. We combined HSC-T with intra-bone delivery of GFP^{+} BMSCs and measured stromal chimerism in the bone by assessing CFU-F activity (Figure S4C). Four weeks after irradiation/transplantation, stromal progenitors were mainly donor-derived in 66% of animals (n = 15) and even at 6 and 9 weeks half of the animals (n = 16 and 2, respectively) had over 50% of their CFU-F activity derived from GFP^{+} donor cells (Figure 5G). At 3 months, the frequency of donor-derived $CD73^{+}$ $CD105^{-}$ $SCA1^{+}$ cells within the recipient BM stroma still reached around 50% of the level found in in age-matched controls (Figure 5H). Furthermore, their differentiated progeny were frequently observed at 12 and 16 weeks (see below). We next determined whether the transplanted stromal progenitor cells expanded in vivo. Since transplantation selects for the $CD73^{+}$ $CD105^{-}$ $SCA1^{+}$ phenotype, we compared the CFU-F within this input population to that re-isolated from the femur 4–9 weeks after transplantation. This revealed that the engrafting BMSC progenitor cells expanded around 6-fold in vivo (n = 28; Figure 5I). Together, this suggested that only a rare $CD73^{+}$ $CD105^{-}$ $SCA1^{+}$ population within the BMSCs engrafted, self-renewed, and produced heterogeneous stromal progeny.

Comparison of Engrafting BMSCs with Other Stromal Populations

In order to molecularly characterize the engrafting stromal cells defined herein and to compare them to known stromal stem and progenitor populations, we performed gene expression analysis of freshly isolated Lin^{-} $CD73^{+}$ $CD105^{-}$ and Lin^{-} $CD73^{+}$ $CD105^{+}$ BMSC populations using Affymetrix MoGeneST1.0 arrays (Figure 6A). Published stromal cell types functionally contributing to HSC niches include $NESTIN^{+}$ and leptin receptor $(LEPR)^{+}$ skeletal stem cells (SSCs), $SP7^{+}$ ($OSTERIX^{+}$) osteoprogenitors, $CXCL12^{+}$ reticular cells, $GFAP^{+}$ non-myelinating Schwann cells, and sinusoidal endothelial cells. Some of these niche cell populations are thought to derive from SSCs. Consequently, we compared the gene expression data from engrafting BMSCs to available microarray data of the above stromal subsets and to data from SSCs isolated using lineage reporter transgenes (*Ebf2*-creERT and *Grem1*-creERT combined with Rosa26-YFP). In order to reduce the complexity of the data, we merged replicates into single profile representatives of the analyzed population and performed hierarchical clustering after correcting for batch effects. This revealed that stromal cells in the bone can be divided into two major branches with few subclusters. SSCs isolated based on *Grem1* and *Ebf2* transgenes clustered closely (Figure 6A). These cells reportedly show full chondrocyte and osteoblast differentiation potential and $EBF2^{+}$

(H) $CD3^{-}CD8a^{-}Gr1^{-}IgM^{-}B220^{int}CD43^{int}CD24^{+}BP1^{-}$ Fraction B, (I) $CD3^{-}CD8a^{-}Gr1^{-}IgM^{-}B220^{int}CD43^{int}CD24^{low}BP1^{+}$ Fraction C, and (J) $CD3^{-}CD8a^{-}Gr1^{-}IgM^{-}B220^{int}CD43^{int}CD24^{high}BP1^{+}$ Fraction C'.

(K) RT-qPCR for B cell lineage differentiation factors expressed in BMSCs from age-matched controls and chimeric mice 4 weeks post-TBI/HSC-T (data pooled from four independent experiments; unpaired parametric t test).

(L) Abundance of $(IgM^{+}/IgD^{+})Gr1^{-}CD11b^{-}B220^{+}CD19^{+}CD93^{+}$ transitional B cells in the spleen of animals treated as described above (representative of two independent experiments with n = 4 or 7 per group; unpaired parametric t test).

(M) Control mice or mice 8 weeks after HSC-T with or without BMSC co-transplantation were immunized with TNP-Ficoll and the change in anti-TNP-specific IgM levels pre- and post-immunization (11 days) was measured by ELISA (three independent experiments with n = 14 for control, n = 18 for HSC-T and n = 20 for HSC-T + BMSC animals; unpaired parametric t test).

See also Figure S3.

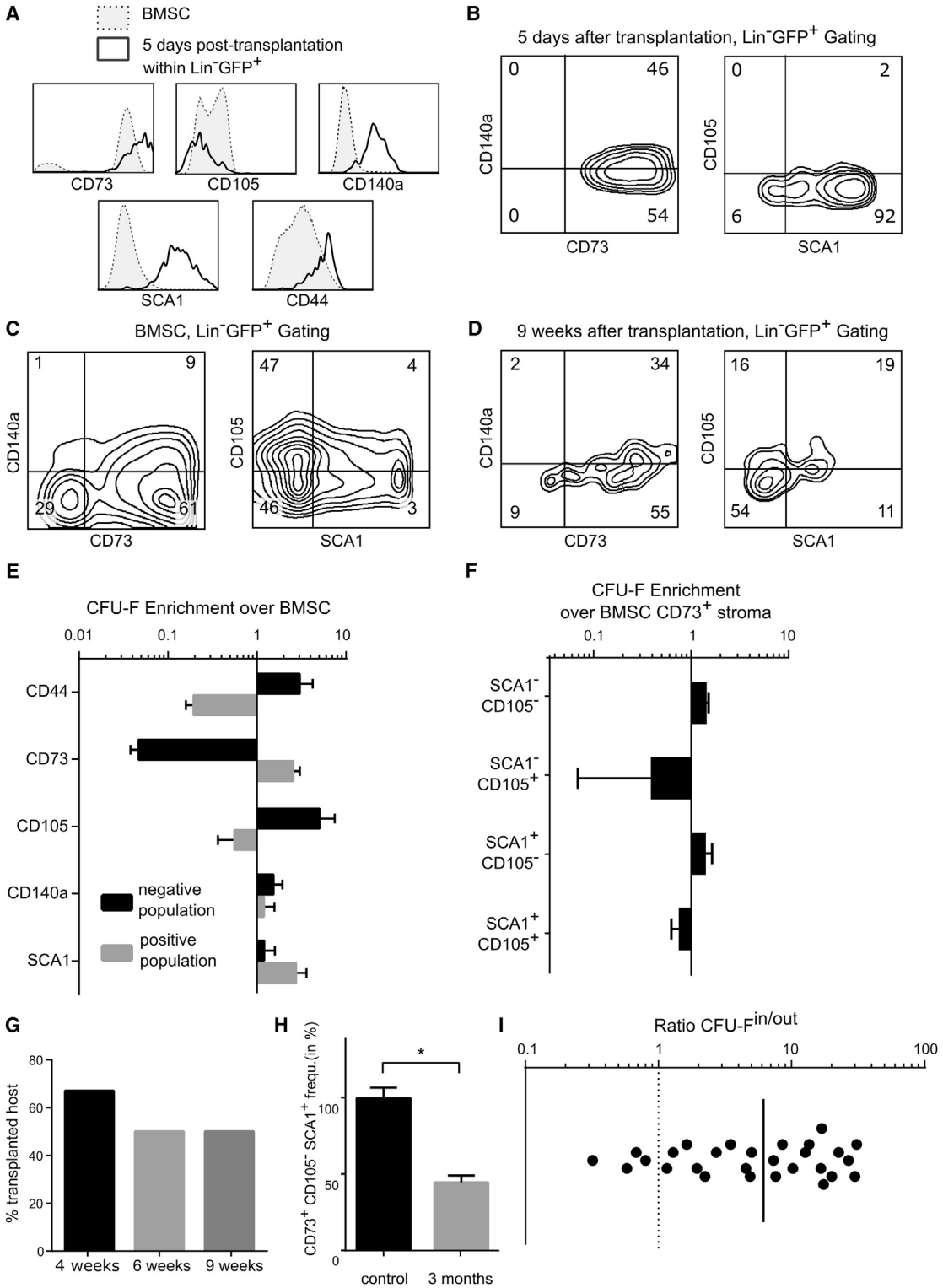

Figure 5. Phenotypic and Functional Characterization of BMSCs

(A–D) Primary Lin$^-$ GFP$^+$ stroma cells were analyzed by flow cytometry for the expression of the indicated cell surface markers. Following transplantation into irradiated recipient mice, engrafted Lin$^-$ GFP$^+$ stroma cells were re-analyzed 5 days (A and B) or 9 weeks later (D). Representative plots from three independent experiments.

(legend continued on next page)

cells were found in close proximity to HSCs. A second, closely related sub-cluster of this branch included the CD73$^+$ CD105$^-$ cells together with pre-BCSPs (bone cartilage and stromal progenitors) and BCSP cells (Figure 6A), two populations with multi-lineage potential producing diverse stromal subsets (Chan et al., 2015). In the second major branch, CD73$^+$ CD105$^+$ clustered with more differentiated populations shown to participate in HSC niches (6C3 = BP-1) and niches for committed hematopoietic lineages (Figure 6A). Interestingly, gene ontology (GO) term enrichment revealed upregulation of genes implicated in endochondral ossification and chondrocyte differentiation in the CD73$^+$ CD105$^-$ population, which is in line with their similarity to BCSPs (Figure 6B). Further, CD73$^+$ CD105$^-$ cells expressed genes involved in cholesterol biosynthesis, which affects HSC proliferation and mobilization (Westerterp et al., 2012). On the other hand, the CD73$^+$ CD105$^+$ population expressed genes implicated in B cell differentiation (Figure 6C), which is reportedly osteoblast driven (Zhu et al., 2007). Altogether, these analyses indicated that Lin$^-$ CD73$^+$ CD105$^-$ cells resembled SSCs and stromal progenitors shown to support HSC homeostasis.

Multipotency of Engrafting BMSC Progenitors

Multi-lineage differentiation potential has been described in clonogenic BM stromal cells and has been linked to stem cell activity in that lineage (Pittenger et al., 1999). We therefore used in vitro functional differentiation assays to determine whether the BMSC subpopulations we had identified exerted multi-lineage differentiation capacity. We evaluated four Lin$^-$ CD73$^+$ BMSC subpopulations (CD73$^+$, CD105$^{+/-}$, and SCA1$^{+/-}$) corresponding to the phenotypes we had observed either shortly after transplantation or after in vivo expansion. Single, flow-sorted cells were plated and clonally expanded for 2 weeks. Cells were then split to assess osteogenic, chondrogenic, and adipogenic lineage differentiation potential (Figure 6D; CD73$^+$ CD105$^+$ SCA1$^-$ cells were excluded since they did not expand). We found that tripotent osteogenesis, chondrogenesis, and adipogenesis differentiation potential was most evident in the CD73$^+$ CD105$^-$ SCA1$^+$ population (Figure 6D). We next addressed the in vivo differentiation potential of transplanted GFP$^+$ BMSCs using immunofluorescence and -histochemistry. Twelve weeks after transplantation, engrafted GFP$^+$ cells were located in the metaphysis region of the bone and had in part differentiated into chondrocytes and OSTERIX$^+$ osteoprogenitors (Figures S5A and S5B). Occasionally, GFP$^+$ cells were observed in the cortical bone, and immunostaining identified them as RUNX2$^+$ osteoblasts (Figure S5C). On the other hand, differentiation into oil red O$^+$ adipocytes was very rare (Figure S5D). Thus, transplanted GFP$^+$ BMSCs exerted multi-lineage differentiation potential in vivo.

Finally, we assessed the engraftment potential of purified BMSC sub-populations. Lin$^-$ CD73$^+$ cells differentially expressing CD105 and SCA1 were isolated by fluorescence-activated cell sorting (FACS) from GFP$^+$ donors and 200 cells were transplanted (intra-femural) into irradiated Insulin-GFP recipients together with GFP$^-$ rescue BM (intra-venous) to ensure hematopoietic reconstitution. After 9 weeks, stromal cells were re-isolated to characterize GFP$^+$ cells (Figure 6E). Robust engraftment was observed using CD73$^+$ CD105$^-$ SCA1$^+$ BMSCs (100% of experiments, n = 4), while the CD73$^+$ CD105$^+$ SCA1$^+$ population engrafted only occasionally (25% of experiments, n = 4), and the two remaining populations did not engraft. Cells re-isolated from CD73$^+$ CD105$^+$ SCA1$^+$ grafts never expanded in vitro, which precluded the analysis of their multi-lineage differentiation potential. In contrast, single cells re-isolated from CD73$^+$ CD105$^-$ SCA1$^+$ grafts expanded in vitro demonstrating their self-renewal potential. In addition, clonal progeny were multipotent as they retained the capacity to differentiate into osteoblast, chondrocyte, and adipocyte lineage cells (Figure S5E; frequency of tripotent clones 67%, n = 4). We concluded that the Lin$^-$ CD73$^+$ CD105$^-$ SCA1$^+$ BMSC sub-population exerted stem-like activity, i.e., had the capacity to engraft, clonally expand, and maintain multi-lineage differentiation potential in vivo.

Engrafted BMSCs Localize Close to HSCs and Increase the Number of HSC Clusters In Vivo

Support of HSC function in the BM relies on local tissue microenvironments/niches composed of mesenchymal stroma and endothelial cells (Méndez-Ferrer et al., 2015). We therefore aimed at analyzing the localization of engrafted GFP$^+$ BMSCs relative to HSCs 16 weeks post-transplantation. We distinguished GFP$^+$ SCA1$^+$ progenitor stromal cells, which have engraftment and multi-lineage differentiation capacity (Figure 6), and their GFP$^+$ SCA1$^-$ progeny, which account for around 90% of stromal cells 16 weeks post-transplantation. Since transplanted HSCs and SCA1$^+$ stromal cells are very rare (0.01‰ and 0.1‰, respectively), we recorded the localization of cells in the entire bone cavity at high resolution. We utilized 3D whole-mount imaging by light-sheet microscopy of decalcified and cleared femurs that were labeled with fluorescent-conjugated antibodies (Figure 7A). Engrafted BMSCs (GFP$^+$) were abundantly present both at the metaphysis and cortical region. Clusters of Lin$^-$ CD150$^+$ CD48$^-$ CD41$^-$ HSCs were in close proximity to GFP$^+$ SCA1$^+$ stromal cells (Figure 7B). In order to quantify these results, we performed automated detection, segmentation, and classification of cells using LoG detectors, B-spline

(E and F) Different stromal sub-populations were purified based on the expression of the indicated markers and evaluated by CFU-F assays. The diagram shows the enrichment (or loss) of CFU-F activity in comparison to Lin$^-$ BM stroma for single markers (E) and relative to CD73$^+$ stroma for marker combinations (F) (n = 3; error bars show SD).

(G and H) TBI/HSC-T was combined with co-transplantation of MACS-enriched GFP$^+$ BMSCs. After 4–9 weeks, the expansion capacity of transplanted stromal progenitors was measured by CFU-F assays (n = 15, 16, and 2 for 4, 6, and 9 weeks, respectively) (G). The engraftment was considered successful if the majority of the resulting colonies was GFP$^+$. Three months after transplantation, the frequency of CD73$^+$ CD105$^-$ SCA1$^+$ BMSCs within the BM stroma was measured by flow cytometry (H) and compared to age-matched, non-irradiated, non-transplanted controls (n = 5 each, unpaired parametric t test; error bars show SD).

(I) The number of CFU-F colonies produced from primary CD73$^+$ CD105$^-$ SCA1$^+$ cells (CFU-F^{in}) was compared to that deriving from these cells 4–9 weeks after transplantation (CFU-F^{out}). This provides a measure for the in vivo expansion of stromal progenitor cells (n = 28).

See also Figure S4.

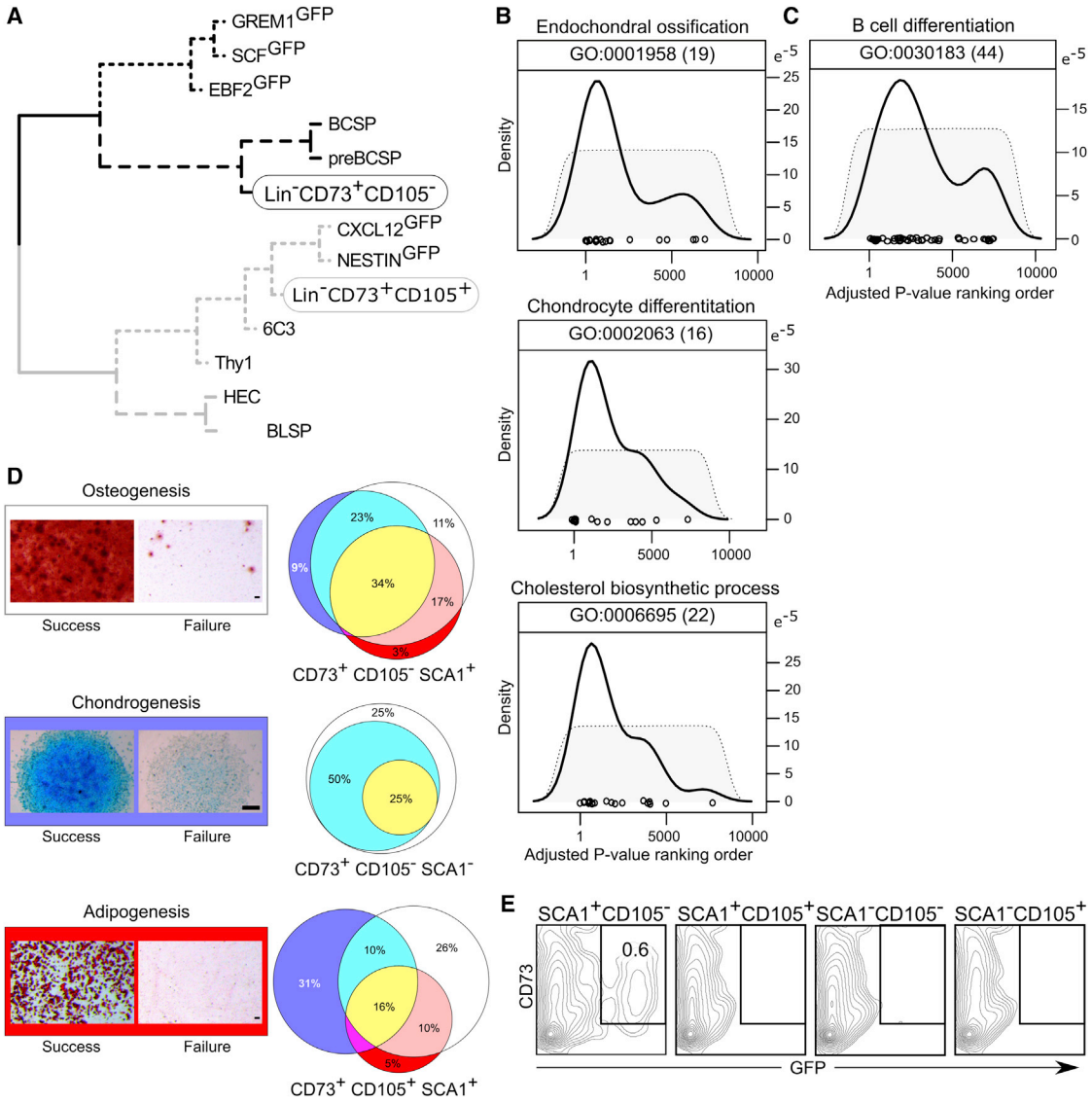

Figure 6. Transcriptome Analysis of Primary CD73$^+$CD105$^-$ Stromal Cells and Their Relation to Known BMSC Populations

(A) Clustering of different stromal populations in the bone marrow based on mRNA expression analysis in order to compare the primary CD73$^+$ CD105$^-$ BM stroma population to known stromal isolates. HEC, hepatic leukemia factor-expressing cells; BLSP, B cell lymphocyte stromal progenitor; BCSP, bone, cartilage stromal progenitor as defined (Chan et al., 2015).

(B and C) Gene set enrichment analysis for genes upregulated in CD73$^+$ CD105$^-$ (B) or CD73$^+$ CD105$^+$ (C) BMSCs revealed significant overlap with the indicated gene ontology (GO) terms. The dotted line shows the background level of enrichment obtained by random gene selection.

(D) Clonally expanded single cells were subjected to in vitro differentiation into osteogenic (white), chondrogenic (blue) and adipogenic (red) cells. Pictures depict representative examples of successful and failed differentiation. Scale bars, 100 μm. The Venn diagrams on the right illustrate the percentage of clones with tri- (yellow), bi-potent (pink or light blue), or single differentiation activity (white, red, and blue) in the indicated subpopulations of BMSCs (36, 8, or 19 clones were analyzed).

(E) Flow cytometry for CD73 and GFP among Lin$^-$ stromal cells 9 weeks after TBI/HSC-T plus co-transplantation with the indicated Lin$^-$ GFP$^+$ CD73$^+$ sub-populations. Robust engraftment was observed only from CD73$^+$ SCA1$^+$ CD105$^-$ cells.

See also Figure S5.

snakes, and Gaussian mixture models, which allowed resolving variations in size, shape, and marker intensity of the different cell types (Figures 7C and S6A). When we compared the distance between SCA1$^+$ or SCA1$^-$ stromal cells and the nearest HSCs (2,356 cells total), we observed a mean distance of 25 μm for SCA1$^+$ GFP$^+$ (2,296 cells total) compared to 83 μm for SCA1$^-$ GFP$^+$ (22,188 cells total) stromal cells (Figure 7D). We used inhomogeneous multi-type pair correlation to calculate the likelihood that two cell types have a certain distance taking into account their respective abundance. This showed that SCA1$^+$ (but not SCA1$^-$) stromal progenitors localized closer to HSCs than predicted by a random Gaussian distribution (Figures 7E and S6B).

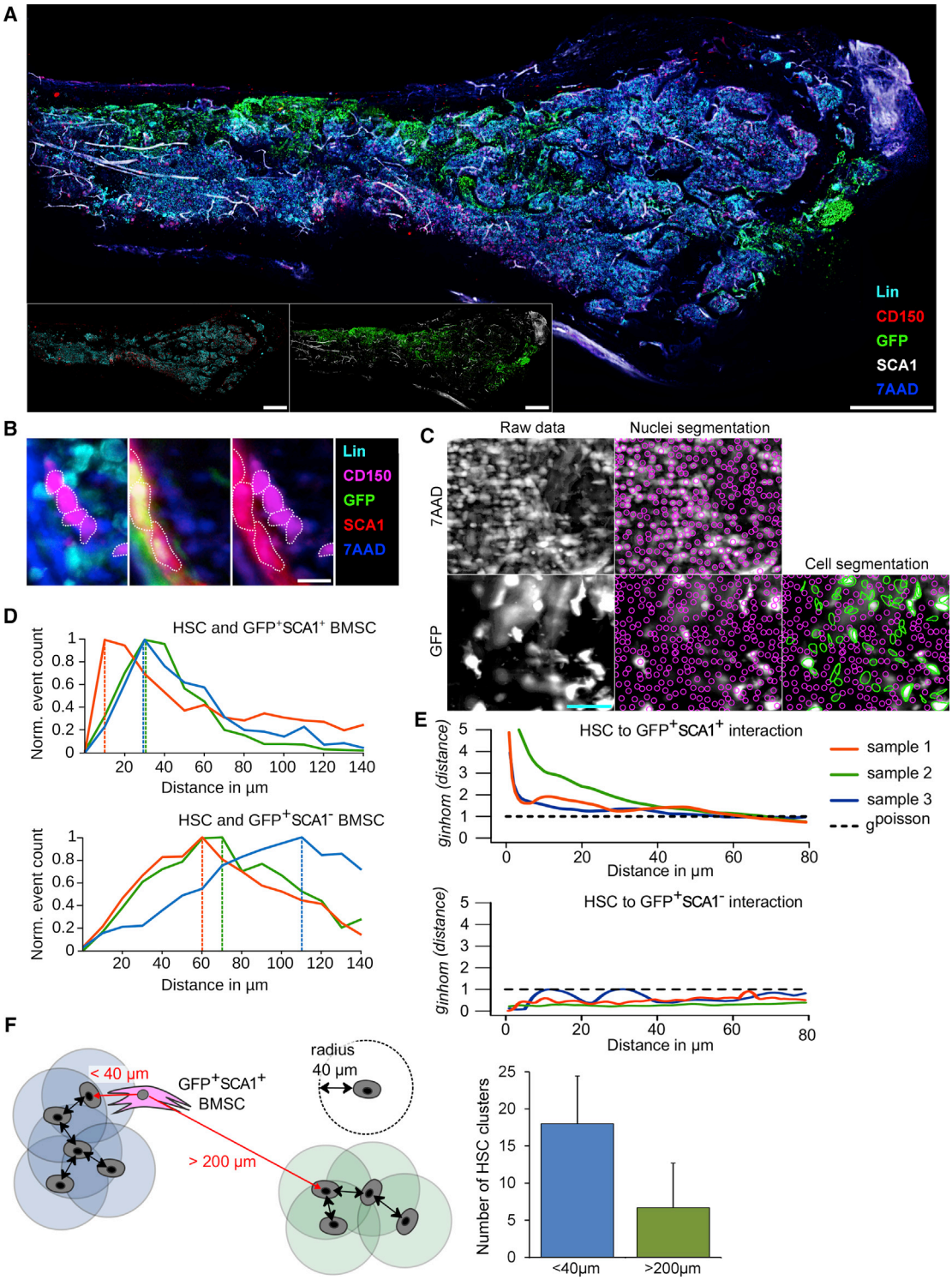

Figure 7. Engrafted GFP$^+$ BMSCs Localize Close to HSCs and Increase the Number of HSC Clusters In Vivo

(A) Whole-mount immunofluorescence of a bone 16 weeks post-transplantation recorded by light-sheet imaging. Engrafted BMSC are shown in green (GFP), the lineage cocktail (Lin) (CD4, CD8, CD11b, CD19, Ter119, Gr-1, CD48, CD41) in cyan, SCA1 in white, CD150 in red, and nuclei in blue. Combination of channels for GFP$^+$ BMSCs and HSCs are shown as insets. Scale bars, 1 mm.

(B) Immunofluorescence imaging showing a cluster of five HSCs (Lin in cyan, CD150 in magenta, nuclei in blue) and transplanted GFP$^+$ SCA1$^+$ BMSC (GFP in green, SCA1 in red, nuclei in blue). Scale bar, 10 µm.

(legend continued on next page)

Clusters of HSCs have been suggested to reflect the existence of local niches supporting HSC self-renewal (Wang et al., 2013). Closely spaced HSCs (four and more HSCs within 40 μm from each other as detected by density-based spatial clustering with Dbscan) were predominantly observed in the vicinity (less than 40 μm, which is the 25th percentile of all distances between all GFP$^+$ SCA1$^+$ cells and all HSCs) of SCA1$^+$ stromal progenitors, but were rare at larger distance (above 200 μm, the 75th percentile of all distances; Figure 7F). Of note, more than half of all HSCs were part of such clusters, and nearly all SCA1$^+$ stromal progenitors were found in these clusters (Figure S6C). In summary, these data supported the concept that co-transplanted stromal progenitors acted locally to support HSC function and expansion. After irradiation/HSC-T, transplanted SCA1$^+$ stromal progenitors localized close to HSCs in line with previous results in the undisturbed bone marrow and were found in niches containing clusters of several HSCs suggestive of short distance, productive interactions between these cell types.

DISCUSSION

Here, we show TBI, which is used to eliminate the host hematopoietic system before HSC-T, severely damages the BM stroma. This constrained HSC maintenance, limited the quantity of HSC, which successfully engrafted and/or expanded, and delayed the recovery of innate and adaptive immunity. Specifically, multipotent BM stroma progenitor cells were lost and failed to recover spontaneously. Their levels stayed below 10% for at least 4 months post-TBI as compared to age-matched untreated controls. Importantly, we found that this deficiency could be corrected by the transplantation of primary BMSCs, which significantly ameliorated the abundance of donor HSCs in irradiated recipients and improved neutropenia and B lymphopoiesis. This indicated that stromal niches represent an important limiting factor for the efficient reconstitution of the hematopoietic system. The stroma does not appear to play a role for the initial homing of HSC after transplantation, since intra-bone injection and intravenous administration of HSC resulted in similar hematopoietic reconstitution and chimerism (van Os et al., 2010). Rather, the stroma seems to be essential for efficient HSC expansion and maintenance.

B cells mediate humoral immunity important to restrict infections and are involved in controlling GvHD. High levels of donor-derived pro-B cells are associated with a significantly decreased incidence of acute GvHD (Michonneau et al., 2009). Likewise, B-cell-derived IL-10 may inhibit the expansion of alloreactive T cells and thus protect from acute GVHD (Rowe et al., 2006). B lymphopoiesis is chiefly supported by osteoblasts (Zhu et al., 2007; Yu et al., 2016) indicating that irradiation induced stromal damage may extend to osteoblasts and thus the skeletal system. This may explain the observation that bone loss and fractures are frequent events for childhood leukemia patients receiving HSC-T (Mostoufi-Moab et al., 2012).

Unfortunately, the ability of BMSCs to support hematopoiesis was rapidly lost when these cells were cultured in vitro. This may be due to a failure of cultured stromal cells to engraft as already described by earlier reports (Rombouts and Ploemacher, 2003). However, as we show now, even direct transplantation of cultured BMSCs by intrafemoral injection did not enhance HSC expansion suggesting additional defects. The massive upregulation of SPP1, a factor known to limit HSC expansion (Stier et al., 2005), that we observed in cultured BMSCs may explain this defect. Rather than supporting HSC, transplantation of cultured BMSCs increased common lymphoid progenitors, which is in line with clinical reports showing that in-vitro-expanded BMSCs elevate lymphocyte numbers (Ball et al., 2007). It remains to be seen why these cultured cells supported disease propagating cells while they failed to support normal HSC.

Importantly, freshly isolated, primary BMSCs engrafted long-term and improved hematopoietic reconstitution. The engrafting, CD73$^+$ CD105$^-$ SCA1$^+$ BMSC sub-population accounted for less than 3% of all BMSCs. For direct application, these cells are therefore too rare. Future analyses of these cells in vivo and ex vivo may help to define alternative expansion conditions, which better preserve the stem and progenitor functions of these cells. As a first step in this direction, we generated gene expression profiles of BMSC progenitors, which will be an important tool for guiding this optimization process. If successful, this may also be useful to expand cord-blood-derived HSCs in vitro.

When comparing the different assays to evaluate BM stroma progenitor phenotype and function, we noticed that a combination of distinct approaches was required to assess the full potential of stromal cells. For example, the CFU-F assay yields colonies from putative progenitors as well as from apparently more differentiated cell types indicating that "clonal expansion" capacity is not sufficient to characterize this type of stem cells. Similarly, differentiation assays are only informative if performed using clonally expanded, single cells. This is not only a pre-requisite to confirm multi-lineage differentiation potential but is also instrumental for measuring small differences in the differentiation capacity of related subpopulations. Finally, transplantation studies in vivo are essential to confirm stem cell behavior. For example, while all sub-populations (divided based on CD105 and SCA1) within the Lin$^-$ CD73$^+$ subset generated colonies in the CFU-F assay, only one of these sub-populations had the capacity to engraft. Thus only a combination of functional assays

(C) Laplacian of Gaussian (LoG) detector for the segmentation of nuclei (top row, 7AAD channel in grayscale with overlapping nuclei in magenta) and B-spline snake segmentation (bottom row, CD150 channel in grayscale with overlapping nuclei in magenta and sdROI in green) as exemplified for a Z-projection of one stack. Scale bar, 30 μm.

(D) Distance between GFP$^+$ SCA1$^+$ (top) or GFP$^+$ SCA1$^-$ (bottom) BMSCs to the nearest Lin$^-$ SCA1$^+$ CD150$^+$ HSCs. Dotted lines mark the most frequent distance between HSCs and GFP$^+$ cells. Each color represents data derived from an individual mouse (n = 3).

(E) Statistical analysis for spatial dependence between point patterns with inhomogeneous density. Ripley correction was used to for anatomic boundaries. Each color represents data derived from an individual mouse (n = 3); dotted black lines represent complete spatial randomness.

(F) Number of HSC clusters in proximity (below 40 μm) or distant (above 200 μm) to GFP$^+$ SCA1$^+$ BMSC. Only clusters with at least four HSC within a neighborhood radius lower than 40 μm were considered. The left panel illustrates the clustering algorithm DBscan (n = 3; error bars show SD).

See also Figure S6.

allowed the definition of a set of markers (Lin$^-$ CD73$^+$ CD105$^-$ SCA1$^+$) to quantitatively isolate BM stromal cells exhibiting all properties associated with stem and progenitor capacity.

CD105 had been reported previously as a marker of skeletal lineage commitment during limb development and was shown to increase during transition from SSCs to BCSPs (Chan et al., 2015). We found the CD73$^+$ CD105$^-$ SCA1$^+$ population to be enriched for multipotency at the clonal level in vitro but were not able to detect significant adipogenic contribution of this population in vivo, in line with other reports (Worthley et al., 2015). Nevertheless, this population showed robust engraftment, mediated long-term stromal reconstitution and supported HSC function. Cells lacking both SCA1 and CD105 were unable to engraft in vivo. A previous study already showed loss of SCA1 within the endosteal osteoblastic compartment (Nakamura et al., 2010) in agreement with preferential Sca1 expression by progenitor cells. Other phenotypes used to describe BMSCs include CD140a$^+$ SCA1$^+$, and such cells showed osteogenic, adipogenic, chondrogenic, and endothelial potential in vitro (Morikawa et al., 2009). However, the experimental design of this study did not exclude cells positive for the endothelial marker CD31, which may explain the observed contribution to the endothelial lineage. We have observed that the majority of BMSCs are CD140a negative, in agreement with another recent study (Li et al., 2014). When CD140a$^+$ SCA1$^+$ SSCs were injected intravenously (i.v.) (retro-orbital), homing to the BM was observed only occasionally, and quantification was not possible (Morikawa et al., 2009). When we performed systemic delivery of BMSCs via intravenous injection, we observed massive trapping of cells in the lung with only very few cells homing to the BM (data not shown).

We now provide a method to study the function of BM stroma stem and progenitor cells and their progeny in their normal environment, which will help to better define their lineage relations, properties, and how they contribute to hematopoiesis. Importantly, transplanted BMSCs co-localize to niches containing clusters of HSCs indicating that the expansion of HSCs following irradiation/transplantation may be due to local interactions between stromal progenitors and HSCs. The exact nature of these interactions is an open question, which will require additional work. The proximity of HSC and BMSC clusters was in good agreement with previous reports on the distance between SSCs and HSCs (Méndez-Ferrer et al., 2010; Kunisaki et al., 2013). This previous examination was done under steady-state conditions, which suggests that transplantation of BMSCs into the irradiated BM is able to re-establish similar niche structures.

Unexpectedly, we observed that HSC numbers still increased when transplantation of BMSCs was delayed. This raises the possibility to correct stromal defects in HSC-T patients with insufficient hematopoietic function. Unfortunately, we find that endogenous mobilization of BM stromal cells is very inefficient, and that BMSCs delivered systemically did not engraft into the bone marrow. Alternative routes of administration such as injections into the iliac and subclavian arteries or the sternum could be evaluated for such patients. Independently, currently used pre-conditioning regimens should be evaluated to identify treatments which best preserve the endogenous stroma. For example, we have observed that reduced intensity conditioning produced less BM stroma damage than TBI in the mouse. Indeed, treatment with cyclophosphamide or cytarabine reduced CFU-F activity by 40% and 25%, respectively, as compared to 95% with TBI (data not shown). This suggests that faster recovery from neutropenia, which has been observed in some RIC regimen, could be due to reduced stromal damage. Current clinical trials using BM stroma transplantation often failed to show benefits, which may be related to differences in cell preparation, expansion, route of administration, and pre-conditioning. We expect that the improved experimental designs established herein will facilitate defining better ways for the therapeutic application of BM stroma in HSC transplantation.

STAR★METHODS

Detailed methods are provided in the online version of this paper and include the following:

- KEY RESOURCES TABLE
- CONTACT FOR REAGENT AND RESOURCE SHARING
- EXPERIMENTAL MODEL AND SUBJECT DETAILS
- METHOD DETAILS
  - Pre-conditioning irradiation
  - Extraction of BM-stromal cells
  - MACS-enrichment of stromal cells
  - BM-stroma cell culture
  - CFU-S Assay
  - CFU-F assay
  - Clonal expansion of BMSC
  - Bone marrow and BM stroma transplantation
  - Multilineage reconstitution assay
  - Hapten immunization and ELISA
  - Osteogenic differentiation
  - Adipogenic differentiation
  - Chondrogenic differentiation
  - RNA extraction and Real-time RT-PCR
  - Immunohistochemistry and immunocytochemistry
  - Gene expression profiling
  - FACS
  - Light-sheet imaging of cleared bone samples
- QUANTIFICATION AND STATISTICAL ANALYSIS
- DATA AND SOFTWARE AVAILABILITY

SUPPLEMENTAL INFORMATION

Supplemental Information includes six figures, one table, and Methods S1 and can be found with this article online at http://dx.doi.org/10.1016/j.stem.2017.07.004.

AUTHOR CONTRIBUTIONS

J.-P.A. and Z.T. performed experiments. J.H. supervised the project. J.-P.A., W.H., and J.H. designed the experiments, analyzed the data, and wrote the manuscript.

ACKNOWLEDGMENTS

J.-P.A., Z.T., W.H., and J.H. were supported in part by grants from the SNF. We thank P. Dessen for excellent technical support, N. Desbaillets, L. Beziaud, and L. Spisak for help with collecting data, D. Sage and V. Uhlmann for support in image processing, P. Briquez for setup of immunohistochemistry, G. Asherton for TNP experiments, and U. Koch and T. Sugrue for help when establishing flow cytometry of HSCs and B cells.

Received: March 25, 2015
Revised: May 8, 2017
Accepted: July 10, 2017
Published: August 3, 2017

REFERENCES

Acar, M., Kocherlakota, K.S., Murphy, M.M., Peyer, J.G., Oguro, H., Inra, C.N., Jaiyeola, C., Zhao, Z., Luby-Phelps, K., and Morrison, S.J. (2015). Deep imaging of bone marrow shows non-dividing stem cells are mainly perisinusoidal. Nature *526*, 126–130.

Anasetti, C., Logan, B.R., Lee, S.J., Waller, E.K., Weisdorf, D.J., Wingard, J.R., Cutler, C.S., Westervelt, P., Woolfrey, A., Couban, S., et al.; Blood and Marrow Transplant Clinical Trials Network (2012). Peripheral-blood stem cells versus bone marrow from unrelated donors. N. Engl. J. Med. *367*, 1487–1496.

Baddeley, A., and Turner, R. (2005). spatstat: An R package for analyzing spatial point patterns. J. Stat. Softw. *12*. Published online January 26, 2005. http://dx.doi.org/10.18637/jss.v012.i06.

Ball, L.M., Bernardo, M.E., Roelofs, H., Lankester, A., Cometa, A., Egeler, R.M., Locatelli, F., and Fibbe, W.E. (2007). Cotransplantation of ex vivo expanded mesenchymal stem cells accelerates lymphocyte recovery and may reduce the risk of graft failure in haploidentical hematopoietic stem-cell transplantation. Blood *110*, 2764–2767.

Bhattacharya, D., Czechowicz, A., Ooi, A.G., Rossi, D.J., Bryder, D., and Weissman, I.L. (2009). Niche recycling through division-independent egress of hematopoietic stem cells. J. Exp. Med. *206*, 2837–2850.

Chan, C.K., Seo, E.Y., Chen, J.Y., Lo, D., McArdle, A., Sinha, R., Tevlin, R., Seita, J., Vincent-Tompkins, J., Wearda, T., et al. (2015). Identification and specification of the mouse skeletal stem cell. Cell *160*, 285–298.

Delgado-Gonzalo, B.R., and Unser, M. (2013). Spline-based framework for interactive segmentation. IEEE Trans. Image Process. *34*, 235–243.

Ding, L., and Morrison, S.J. (2013). Haematopoietic stem cells and early lymphoid progenitors occupy distinct bone marrow niches. Nature *495*, 231–235.

Ding, L., Saunders, T.L., Enikolopov, G., and Morrison, S.J. (2012). Endothelial and perivascular cells maintain haematopoietic stem cells. Nature *481*, 457–462.

Domenech, J., Linassier, C., Gihana, E., Dayan, A., Truglio, D., Bout, M., Petitdidier, C., Delain, M., Petit, A., Brémond, J.L., et al. (1995). Prolonged impairment of hematopoiesis after high-dose therapy followed by autologous bone marrow transplantation. Blood *85*, 3320–3327.

Greenbaum, A., Hsu, Y.M., Day, R.B., Schuettpelz, L.G., Christopher, M.J., Borgerding, J.N., Nagasawa, T., and Link, D.C. (2013). CXCL12 in early mesenchymal progenitors is required for haematopoietic stem-cell maintenance. Nature *495*, 227–230.

Iscove, N.N., and Nawa, K. (1997). Hematopoietic stem cells expand during serial transplantation in vivo without apparent exhaustion. Curr. Biol. *7*, 805–808.

Itkin, T., Gur-Cohen, S., Spencer, J.A., Schajnovitz, A., Ramasamy, S.K., Kusumbe, A.P., Ledergor, G., Jung, Y., Milo, I., Poulos, M.G., et al. (2016). Distinct bone marrow blood vessels differentially regulate haematopoiesis. Nature *532*, 323–328.

Jaqaman, K., Loerke, D., Mettlen, M., Kuwata, H., Grinstein, S., Schmid, S.L., and Danuser, G. (2008). Robust single-particle tracking in live-cell time-lapse sequences. Nat. Methods *5*, 695–702.

Jones, E., Oliphant, T., Peterson, P., and others (2001). SciPy: Open Source Scientific Tools for Python. http://wwwscipyorg/.

Ke, M.T., Fujimoto, S., and Imai, T. (2013). SeeDB: A simple and morphology-preserving optical clearing agent for neuronal circuit reconstruction. Nat. Neurosci. *16*, 1154–1161.

Kunisaki, Y., Bruns, I., Scheiermann, C., Ahmed, J., Pinho, S., Zhang, D., Mizoguchi, T., Wei, Q., Lucas, D., Ito, K., et al. (2013). Arteriolar niches maintain haematopoietic stem cell quiescence. Nature *502*, 637–643.

Li, H., Ghazanfari, R., Zacharaki, D., Ditzel, N., Isern, J., Ekblom, M., Méndez-Ferrer, S., Kassem, M., and Scheding, S. (2014). Low/negative expression of PDGFR-α identifies the candidate primary mesenchymal stromal cells in adult human bone marrow. Stem Cell Reports *3*, 965–974.

Majhail, N.S., Rizzo, J.D., Lee, S.J., Aljurf, M., Atsuta, Y., Bonfim, C., Burns, L.J., Chaudhri, N., Davies, S., Okamoto, S., et al.; Center for International Blood and Marrow Transplant Research (CIBMTR); American Society for Blood and Marrow Transplantation (ASBMT); European Group for Blood and Marrow Transplantation (EBMT); Asia-Pacific Blood and Marrow Transplantation Group (APBMT); Bone Marrow Transplant Society of Australia and New Zealand (BMTSANZ); East Mediterranean Blood and Marrow Transplantation Group (EMBMT); Sociedade Brasileira de Transplante de Medula Ossea (SBTMO) (2012). Recommended screening and preventive practices for long-term survivors after hematopoietic cell transplantation. Hematol. Oncol. Stem Cell Ther. *5*, 1–30.

Méndez-Ferrer, S., Michurina, T.V., Ferraro, F., Mazloom, A.R., Macarthur, B.D., Lira, S.A., Scadden, D.T., Ma'ayan, A., Enikolopov, G.N., and Frenette, P.S. (2010). Mesenchymal and haematopoietic stem cells form a unique bone marrow niche. Nature *466*, 829–834.

Méndez-Ferrer, S., Scadden, D.T., and Sánchez-Aguilera, A. (2015). Bone marrow stem cells: Current and emerging concepts. Ann. N Y Acad. Sci. *1335*, 32–44.

Michonneau, D., Peffault de Latour, R., Porcher, R., Robin, M., Benbunan, M., Rocha, V., Ribaud, P., Ferry, C., Devergie, A., Vanneaux, V., et al. (2009). Influence of bone marrow graft B lymphocyte subsets on outcome after HLA-identical sibling transplants. Br. J. Haematol. *145*, 107–114.

Morikawa, S., Mabuchi, Y., Kubota, Y., Nagai, Y., Niibe, K., Hiratsu, E., Suzuki, S., Miyauchi-Hara, C., Nagoshi, N., Sunabori, T., et al. (2009). Prospective identification, isolation, and systemic transplantation of multipotent mesenchymal stem cells in murine bone marrow. J. Exp. Med. *206*, 2483–2496.

Mostoufi-Moab, S., Ginsberg, J.P., Bunin, N., Zemel, B., Shults, J., and Leonard, M.B. (2012). Bone density and structure in long-term survivors of pediatric allogeneic hematopoietic stem cell transplantation. J. Bone Miner. Res. *27*, 760–769.

Nakamura, Y., Arai, F., Iwasaki, H., Hosokawa, K., Kobayashi, I., Gomei, Y., Matsumoto, Y., Yoshihara, H., and Suda, T. (2010). Isolation and characterization of endosteal niche cell populations that regulate hematopoietic stem cells. Blood *116*, 1422–1432.

Norlin, A.C., Sairafi, D., Mattsson, J., Ljungman, P., Ringdén, O., and Remberger, M. (2008). Allogeneic stem cell transplantation: Low immunoglobulin levels associated with decreased survival. Bone Marrow Transplant. *41*, 267–273.

Pedregosa, F., Varoquaux, G., Gramfort, A., Michel, V., Thirion, B., Grisel, O., Blondel, M., Prettenhofer, P., Weiss, R., Dubourg, V., et al. (2011). Scikit-learn: Machine learning in Python. J. Mach. Learn. Res. *12*, 2825–2830.

Pittenger, M.F., Mackay, A.M., Beck, S.C., Jaiswal, R.K., Douglas, R., Mosca, J.D., Moorman, M.A., Simonetti, D.W., Craig, S., and Marshak, D.R. (1999). Multilineage potential of adult human mesenchymal stem cells. Science *284*, 143–147.

Pulsipher, M.A., Chitphakdithai, P., Logan, B.R., Leitman, S.F., Anderlini, P., Klein, J.P., Horowitz, M.M., Miller, J.P., King, R.J., and Confer, D.L. (2009). Donor, recipient, and transplant characteristics as risk factors after unrelated donor PBSC transplantation: Beneficial effects of higher CD34+ cell dose. Blood *114*, 2606–2616.

Qian, H., Badaloni, A., Chiara, F., Stjernberg, J., Polisetti, N., Nihlberg, K., Consalez, G.G., and Sigvardsson, M. (2013). Molecular characterization of prospectively isolated multipotent mesenchymal progenitors provides new insight into the cellular identity of mesenchymal stem cells in mouse bone marrow. Mol Cell Biol. *33*, 661–677.

Rombouts, W.J., and Ploemacher, R.E. (2003). Primary murine MSC show highly efficient homing to the bone marrow but lose homing ability following culture. Leukemia *17*, 160–170.

Rowe, V., Banovic, T., MacDonald, K.P., Kuns, R., Don, A.L., Morris, E.S., Burman, A.C., Bofinger, H.M., Clouston, A.D., and Hill, G.R. (2006). Host

B cells produce IL-10 following TBI and attenuate acute GVHD after allogeneic bone marrow transplantation. Blood *108*, 2485–2492.

Sezer, O., Possinger, K., Metzner, B., Illiger, H.J., Wattad, M., Heit, W., Fuss, H., and Schultze, W. (2000). Optimal CD34(+) cell dose in autologous peripheral-blood stem-cell transplantation. J. Clin. Oncol. *18*, 3319–3320.

Stier, S., Ko, Y., Forkert, R., Lutz, C., Neuhaus, T., Grünewald, E., Cheng, T., Dombkowski, D., Calvi, L.M., Rittling, S.R., and Scadden, D.T. (2005). Osteopontin is a hematopoietic stem cell niche component that negatively regulates stem cell pool size. J. Exp. Med. *201*, 1781–1791.

Storek, J., Geddes, M., Khan, F., Huard, B., Helg, C., Chalandon, Y., Passweg, J., and Roosnek, E. (2008). Reconstitution of the immune system after hematopoietic stem cell transplantation in humans. Semin. Immunopathol. *30*, 425–437.

Tomita, Y., Sachs, D.H., and Sykes, M. (1994). Myelosuppressive conditioning is required to achieve engraftment of pluripotent stem cells contained in moderate doses of syngeneic bone marrow. Blood *83*, 939–948.

van Os, R., Ausema, A., Dontje, B., van Riezen, M., van Dam, G., and de Haan, G. (2010). Engraftment of syngeneic bone marrow is not more efficient after intrafemoral transplantation than after traditional intravenous administration. Exp. Hematol. *38*, 1115–1123.

Wang, L., Benedito, R., Bixel, M.G., Zeuschner, D., Stehling, M., Sävendahl, L., Haigh, J.J., Snippert, H., Clevers, H., Breier, G., et al. (2013). Identification of a clonally expanding haematopoietic compartment in bone marrow. EMBO J. *32*, 219–230.

Watanabe, K., Ueno, M., Kamiya, D., Nishiyama, A., Matsumura, M., Wataya, T., Takahashi, J.B., Nishikawa, S., Nishikawa, S., Muguruma, K., and Sasai, Y. (2007). A ROCK inhibitor permits survival of dissociated human embryonic stem cells. Nat. Biotechnol. *25*, 681–686.

Westerterp, M., Gourion-Arsiquaud, S., Murphy, A.J., Shih, A., Cremers, S., Levine, R.L., Tall, A.R., and Yvan-Charvet, L. (2012). Regulation of hematopoietic stem and progenitor cell mobilization by cholesterol efflux pathways. Cell Stem Cell *11*, 195–206.

Wingard, J.R., Majhail, N.S., Brazauskas, R., Wang, Z., Sobocinski, K.A., Jacobsohn, D., Sorror, M.L., Horowitz, M.M., Bolwell, B., Rizzo, J.D., and Socié, G. (2011). Long-term survival and late deaths after allogeneic hematopoietic cell transplantation. J. Clin. Oncol. *29*, 2230–2239.

Worthley, D.L., Churchill, M., Compton, J.T., Tailor, Y., Rao, M., Si, Y., Levin, D., Schwartz, M.G., Uygur, A., Hayakawa, Y., et al. (2015). Gremlin 1 identifies a skeletal stem cell with bone, cartilage, and reticular stromal potential. Cell *160*, 269–284.

Wu, J.Y., Purton, L.E., Rodda, S.J., Chen, M., Weinstein, L.S., McMahon, A.P., Scadden, D.T., and Kronenberg, H.M. (2008). Osteoblastic regulation of B lymphopoiesis is mediated by Gsα-dependent signaling pathways. Proc. Natl. Acad. Sci. USA *105*, 16976–16981.

Yu, V.W., Lymperi, S., Oki, T., Jones, A., Swiatek, P., Vasic, R., Ferraro, F., and Scadden, D.T. (2016). Distinctive mesenchymal-parenchymal cell pairings govern B cell differentiation in the bone marrow. Stem Cell Reports *7*, 220–235.

Zhu, J., Garrett, R., Jung, Y., Zhang, Y., Kim, N., Wang, J., Joe, G.J., Hexner, E., Choi, Y., Taichman, R.S., and Emerson, S.G. (2007). Osteoblasts support B-lymphocyte commitment and differentiation from hematopoietic stem cells. Blood *109*, 3706–3712.

STAR★METHODS

KEY RESOURCES TABLE

REAGENT or RESOURCE	SOURCE	IDENTIFIER
Antibodies		
Biotin anti-mouse CD45 antibody	BioLegend	AB_312968
Biotin anti-mouse CD31 antibody	BioLegend	AB_312910
Biotin anti-mouse TER-119/Erythroid Cells antibody	BioLegend	AB_313704
Biotin anti-mouse/human CD11b antibody	BioLegend	AB_312786
Biotin anti-mouse CD4 antibody	BioLegend	AB_312710
Alexa Fluor(R) 700 anti-mouse CD19 antibody	BioLegend	AB_493734
PerCP anti-mouse Ly-6G/Ly-6C (Gr-1) antibody	BioLegend	AB_893560
PerCP anti-mouse CD3a antibody	BioLegend	AB_893319
PerCP anti-mouse CD8a antibody	BioLegend	AB_893427
Alexa Fluor(R) 700 anti-mouse/human CD45R/B220 antibody	BioLegend	AB_493716
Brilliant Violet 605(TM) anti-mouse IgM antibody	BioLegend	AB_2563358
BV421 anti-mouse CD43 (S7)	BD Biosciences	AB_2665409
PE anti-mouse Ly-51 antibody	BioLegend	AB_313364
PE/Cy7 anti-mouse CD24 antibody	BioLegend	AB_756047
Brilliant Violet 711(TM) anti-mouse IgD antibody	BioLegend	AB_2563342
Brilliant Violet 605(TM) anti-mouse IgM antibody	BioLegend	AB_2563358
Biotin anti-mouse Ly-6G/Ly-6C (Gr-1) antibody	BioLegend	AB_313368
Streptavidin-TexasRed	Thermo Fisher	S6370
APC anti-mouse CD19 antibody	BioLegend	AB_313646
PE/Cy7 anti-mouse CD23 antibody	BioLegend	AB_2103037
Anti-Mouse CD21/CD35 eFluor 450	Thermo Fisher Scientific	AB_2016634
PE anti-mouse CD93 (AA4.1, early B lineage) antibody	BioLegend	AB_1967094
PE anti-mouse CD34 antibody	BioLegend	AB_2629647
APC/Cy7 anti-mouse CD117 (c-kit) antibody	BioLegend	AB_1626280
PE/Cy7 anti-mouse Ly-6A/E (Sca-1) antibody	BioLegend	AB_493597
CD48 Monoclonal Antibody (HM48-1), eFluor 450, eBioscience	Thermo Fisher Scientific	AB_11150972
APC anti-mouse CD150 (SLAM) antibody	BioLegend	AB_493461
PE anti-mouse/human CD45R/B220 antibody	BioLegend	AB_312992
APC anti-mouse CD3 antibody	BioLegend	AB_2561455
PE anti-mouse/human CD44 antibody	BioLegend	AB_312958
PE anti-mouse CD73 antibody	BioLegend	AB_2154094
APC anti-mouse CD105 Antibody	BioLegend	AB_2277915
APC anti-mouse CD140a antibody	BioLegend	AB_2043969
Biotin anti-mouse CD41 antibody	BioLegend	AB_2572133
TruStain fcX(TM) (anti-mouse CD16/32) antibody	BioLegend	AB_1574973
Purified Mouse IgM, κ Isotype Control	BD Biosciences	AB_2665411
Anti-Mouse IgM-Alkaline Phosphatase antibody produced in goat	Sigma	AB_258472
RUNX2 Antibody	Novus	AB_11017079
Goat anti-GFP	Abcam	AB_305643
Sp7 / Osterix antibody	Abcam	AB_2194492
Chemicals, Peptides, and Recombinant Proteins		
TNP-AECM-Ficoll	Biosearch Technologies	F-1300-10
TNP-Ovalbumin	Biosearch Technologies	T-5051-10

(*Continued on next page*)

Continued

REAGENT or RESOURCE	SOURCE	IDENTIFIER
4-Nitrophenyl phosphate disodium salt hexahydrate	Sigma	N2765
Y-27632 dihydrochloride	Sigma	Y0503
Collagenase for general use, Type I	Sigma	C0130
Human TGF beta-3 Recombinant Protein	GIBCO	RP-8600
L-Ascorbic acid 2-phosphate sesquimagnesium salt hydrate	Sigma	A8960
Dexamethasone-Water Soluble	Sigma	D2915
Alcian Blue 8GX	Sigma	A5268
L-Proline	Sigma	P0380
Insulin solution human	Sigma	I9278
3-isobutyl-1-methylxanthine	Sigma	I5879
Oil red O	Sigma	O0625
β-Glycerol phosphate disodium salt pentahydrate	Sigma	50020
Alizarin Red S	Sigma	A5533
Silver Nitrate	Sigma	209139
Crystal violet	Sigma	C0775
Anti-Biotin MicroBeads	Miltenyi Biotec	130-090-485
Deposited Data		
Expression profiling data of BMSC	This paper	GEO: GSE79091
Molecular characterization of prospectively isolated multipotent mesenchymal progenitors provides new insight into the cellular identity of mesenchymal stem cells in mouse bone marrow. Mol Cell Biol 2013 Feb;33(4):661-77.	Qian et al., 2013	GEO: GSE51608
CXCL12 in early mesenchymal progenitors is required for hematopoietic stem-cell maintenance. Nature 2013 Mar 14;495(7440):227-30	Greenbaum et al., 2013	GEO: GSE43613
Mesenchymal and hematopoietic stem cells form a unique bone marrow niche. Nature 2010 Aug 12;466(7308):829-34	Méndez-Ferrer et al., 2010	GEO: GSE21941
Gremlin 1 identifies a skeletal stem cell with bone, cartilage, and reticular stromal potential. Cell 2015 Jan 15;160(1-2):269-84	Worthley et al., 2015	GEO: GSE57729
Endothelial and perivascular cells maintain hematopoietic stem cells. Nature 2012 Jan 25;481(7382):457-62.	Ding et al., 2012	GEO: GSE33158
Identification and specification of the mouse skeletal stem cell. Cell 2015 Jan 15;160(1-2):285-98.	Chan et al., 2015	GEO: GSE64447
Experimental Models: Organisms/Strains		
Tg(Ins1-EGFP)1Hara	MGI	RRID:MGI:3704927
C57BL/6-Tg(CAG-EGFP)1Osb/J	MGI	RRID:IMSR_JAX:003291
Oligonucleotides		
please see Table S1	This paper	NA
Software and Algorithms		
Fast parametric active contour for segmenting nearly elliptic objects	R. Delgado-Gonzalo, M. Unser	http://bigwww.epfl.ch/algorithms/esnake/
Aroma Framework analysis	Henrik Bengtsson	http://aroma-project.org/
Other		
Image analysis	J-P Abbuehl	https://github.com/jpabbuehl/SSC_lightsheetAnalysis
Microarray meta-analysis	J-P Abbuehl	https://github.com/jpabbuehl/SSC_arrayAnalysis

CONTACT FOR REAGENT AND RESOURCE SHARING

Further information and requests for resources and reagents should be directed to and will be fulfilled by the Lead Contact, Joerg Huelsken (joerg.huelsken@epfl.ch).

EXPERIMENTAL MODEL AND SUBJECT DETAILS

We used Insulin-GFP (C57Bl6.Cg-Tg(Ins1-EGFP)1Hara/QtngJ) and beta-actin-GFP (AGFP; ByJ.B6-Tg(CAG-EGFP)1Osb/J) mice which were backcrossed for 15 generations into the FVB background. Animals were housed in barrier units where users must decontaminate, change for single use overalls and shoes, and wear head caps, masks and gloves. All material (cages, bedding and water bottles) was washed with an acidic detergent and autoclaved before entering the facility. Animals were housed in ventilated IVC cages from Tecniplast which were over-pressurized relative to the housing rooms which were again over-pressurized compared to the outside. Climate was controlled at 21°C with a 12h light/dark cycle. Manipulation of animals is done within sterile laminar flows, and in-between cages gloves are disinfected with Virkon S. Animals were monitored daily by caretakers, researchers and expert veterinarians. The used bedding was Aspen Tapvei, diet was 3242 (irradiated) from Provimi-Kliba and water was acidified (pH between 2.5 to 3) on a Prominent CH system resin column; food and water was provided ad libitum. Nesting material and cardboard tunnels were provided and animals were grouped with up to 5 animals of the same sex in one cage. General health monitoring of the colony was performed quarterly according to FELASA recommendations (serology, parasitology, bacteriology) with further tests for Norovirus, *Helicobacter*, Parvovirus, and Minute Virus.

All animal experiments were approved by the cantonal veterinary office and were conducted under federal guidelines for the use and care of laboratory animals. Before starting any experiment, each animal was attributed a new anonymous ID without any attached experimental details. In all experiments, groups were always set with sex-matched and age-matched animals. Allocation to experimental groups was randomized between littermates and cages without altering animal location; order of treatments and assessments was per cage. Adverse events in health monitoring of animals required sacrifice and exclusion from analysis. Genotyping was repeated after sacrifice of the animals and when not confirmed led to exclusion of the respective animal. All experiments were performed during daytime. Additional detail regarding individual animal experiments is provided in the STAR Methods.

METHOD DETAILS

Pre-conditioning irradiation

For all irradiation procedures unless specified differently, animals were irradiated at 9 Gy (2× 4.5 Gy split-dose 4 hr apart) the day before starting the experiment and maintained with Bactrim and Dafalgan in the drinking water ad libitum for 2 weeks.

Extraction of BM-stromal cells

6-8 week old male FVB mice were sacrificed by CO_2 and their femurs were cleaned from muscles and crushed gently in a mortar to release bone marrow cells. BM cells in suspensions were collected and filtered with a 45 μm strainer (BD Falcon) and resuspended in 2% FBS. For extraction of cells from bone matrix, the bone pieces were washed in PBS and incubated at RT for 5 min in 3% collagenase/PBS (Sigma-Aldrich). The pieces were further chopped into ~2 mm fragments and both supernatants and fragments were transferred with 5 mL of Collagenase solution into a 50 mL tube. The tubes were incubated in a shaker at 37°C for 45 min. Once digested, the bones fragments were resuspended with cold 5% FBS (PAA) and filtered through a 100 μm strainer (BD Falcon). Spleens were dissected from the abdominal cavity and filtered through a 40-μm nylon strainer to obtain a single-cell suspension.

MACS-enrichment of stromal cells

BM-stromal cells isolated from the bone matrix were labeled with CD45-biotin, CD31-biotin, CD11b-biotin and Ter119-biotin in 2% FBS for 30 min on ice. After washing, cells were resuspended into MACS Buffer (PBS, 0.5% BSA, 2mM EDTA) and incubated with anti-biotin microbeads (Miltenyi Biotec). After 20 min at 4°C, the sample was rinsed and resuspended at 10^8 cells/ml. The purification was done by the AutoMACS Pro (Miltenyi Biotec).

BM-stroma cell culture

The culture medium consisted of high-glucose DMEM (In*vitro*gen), 9% fetal bovine serum (Brunschwig), 9% horse serum (Hyclone) and 1% penicillin/streptomycin (In*vitro*gen). Cells were plated on normal cell culture dishes (TPP), and cultured at 37°C and 7% CO_2. The medium was changed 3 times per week and cells were harvested after 14 days of culture.

CFU-S Assay

For each transplanted mouse, two sex-matched Actin-GFP mice were irradiated at 5Gy and 24 hr later injected with 60000 BM cells. 12 days later, spleens were fixed in Tellyesniczky solution (70% Ethanol, 5% Formalin, 5% Glacial acetic acid in water) for 2 hr at 4°C and colonies were counted with a stereomicroscope. The average number of duplicates was calculated for each tested BM sample.

CFU-F assay

The CFU-F assay was performed by plating 20'000 cells (from unfractionated BM-stromal cell preparation) and 2'000 cells (from MACS-enriched BM-stromal cell preparation) in a 10 cm dish plate. After 14 days, the wells were washed once with PBS and then stained with 0.5% crystal violet solution (Sigma) for 5 min at RT. After washing, colonies with more than 50 spindle-shaped cells per colony were counted and the CFU-F frequency was calculated by dividing the number of colonies by the number of cells initially plated.

Clonal expansion of BMSC

FACS-enriched BMSC were plated at 0,7 cell/well in collagen-coated (HBSS, 100 μg/ml BSA, 20 mM HEPES pH6.5, 1% *Vitro*gen100 collagen (CellTrix) and filtered at 0,2 μm) 96 well plates and expanded in a hypoxic incubator at 1% 0_2 in BM-stromal cell medium supplemented with 5 mM N-Acetylcysteine. After 1 week, proliferating clones were transferred into collagen-coated 6 well plates and expanded for another week. At 80% confluence, clones were resuspended, counted and tested for their differentiation potential. Differentiation potential of clones for each population that could at least differentiate into one mesenchymal lineage was represented in Venn Diagram Plotter (Pan-Omics)

Bone marrow and BM stroma transplantation

For bone marrow transplantations, cells prepared from bone marrow suspensions were passed through a 40 μm cell strainer, resuspended at 50 million cells per ml in HBSS and 5 million cells were injected intravenously per mouse. For this, animals were prewarmed with an infra- red lamp and injected in the tail vein with cells suspended in a volume of 100 μL using a 1ml Insulin-G Syringe. For BMSC transplantations, cells were suspended in a minimal volume of HBSS supplemented with 10 μM Y-27632 (Sigma) and 10000 cells were injected in a volume of 3 μL using a Hamilton syringe 700RN through the patellar surface into the femur of mice anesthetized with 10mg/kg xylazine and 100mg/kg ketamine. For FAC-sorted stromal population, 200 cells were injected intrafemorally. After operation, the same volume was plated to determine retrospectively the CFU-F amount injected.

For all experiments except for the quantification of HSC expansion, GFP^+ stromal cell cells were derived from Actin-GFP donors and rescuing GFP^- hematopoietic BM cells from Insulin-GFP donors. In contrast for quantification of HSC expansion, GFP^- stromal cells were derived from Insulin-GFP donors and GFP^+ hematopoietic BM cells from Actin-GFP donors. In all experiments Insulin-GFP recipients were used. Four weeks later, cells from both femurs were isolated by flushing the bone marrow and by collagenase treatment of the bone fragments, combined, counted and directly stained for flow cytometry analysis. For all comparative experiments, mice were age- and sex-matched.

Multilineage reconstitution assay

2.5 million GFP^+ BM cells for each tested sample were mixed with 2.5 million GFP^- BM competitor cells from insulin-GFP donors. For all transplants within an experimental series the same GFP^- competitor material was used. Insulin-GFP recipients were irradiated at 9 Gy (single dose) 24h before injection and their blood (after red blood cell lysis) was analyzed by flow cytometry after 4, 8 and 16 weeks for CD3, B220 and Gr-1. Lineage reconstitution was monitored within the GFP^+ population for acquisition of combinations of various lineage-specific markers.

Hapten immunization and ELISA

Control or HSC/HSC+BMSC transplanted mice were immunized i.p. with 10μg TNP-AECM-Ficoll (Biosearch Technologies) in endotoxin-free PBS (Invitrogen) and IgM antibodies specific for TNP were measured in pre- and post-immune (11 days) serum. For ELISA, 1.5μg of TNP-Ova (Biosearch Technologies) was immobilized in MaxiSorp 96 well plates (Thermo Scientific), rabbit α-mouse IgM secondary antibody coupled to alkaline phosphatase (Sigma, diluted 1:10000) and 4-Nitrophenyl phosphate disodium salt hexahydrate was used for detection and purified mouse IgM (Becton Dickinson G155-228) served as a standard.

Osteogenic differentiation

5'000 FACS-enriched BMSC were plated on a 6 well plate (TPP) and expanded for 5 days before differentiation. Osteogenesis medium was used for 21 days with 3 medium changes weekly. It is composed of high-glucose DMEM (In*vitro*gen), 10% FBS (PAA), 1% P/S (In*vitro*gen), 10 mM β-glycerol phosphate (Sigma), 50 μg/mL ascorbic acid-2-phosphate (Sigma) and 10 nM dexamethasone (Sigma). Osteoblast staining was performed with the Von Kossa method and Alizarin Red S.

Adipogenic differentiation

5'000 FACS-enriched BMSC were plated on a 6 well plate (TPP) and expanded for 5 days before differentiation. Adipogenesis medium was used for 21 days with 3 medium changes weekly. It is composed of high-glucose DMEM (In*vitro*gen), 10% FBS (PAA), 1% P/S (In*vitro*gen), 20 μg/mL insulin (Sigma), 100 nM dexamethasone (Sigma), 0.5 μM 3-isobutyl-1-methylxanthine (Sigma, I5879-250MG) and 100 μM indomethacin (Sigma). Adipocytes were fixed in 4% PFA for 1 hr, washed in 60% isopropanol and stained with Oil Red O (2 mg/ml in 60% isopropanol) for 20 min at room temperature.

Chondrogenic differentiation

10‘000 FACS-enriched BMSC were resuspended in 10 μl of chondrogenic medium and transferred into individual wells of a 24 well plate. Following 3 hr for attachment, additional medium was added to cover the well. Medium was changed every 3 days for 3 weeks. The medium is composed of high-glucose DMEM (In*vitro*gen), 1% ITS plus premix (Becton Dickinson), 20 ng/mL recombinant TGF-β3 (GIBCO), 40 μg/mL proline (Sigma), 50 μg/mL ascorbic acid-2-phosphate (Sigma) and 100 nM dexamethasone (Sigma). Chondrocyte staining was done with Alcian blue (10 mg/ml Alcian Blue 8-GX in 0.1 N HCl pH1) overnight followed by a brief wash with 6M Guanidine hydrochloride.

RNA extraction and Real-time RT-PCR

RNA was prepared using a miniRNA kit (QIAGEN) with on-column DNA digestion (QIAGEN). Complementary DNAs were generated using oligo-dT(V) priming and quantitative PCR was performed in triplicates in a StepOnePlus thermocycler (Applied Biosystems) using the Power SYBR green PCR Master Mix (Applied Biosystems). The selected housekeeping gene is Tubulin *Tubb2c*. Amplified transcripts were validated by agarose gel electrophoresis after restriction enzyme digestion. Raw data were analyzed according to the deltaC(T) method.

Immunohistochemistry and immunocytochemistry

Femurs were fixed at 4°C in 4% PFA overnight, decalcified for three days in 0.5 mM EDTA in PBS and washed extensively in distilled water prior to cryo-freezing. Cryosections were permeabilized with 0.1% Triton in PBS for 15 min. After washing in PBS, blocking was done with 3% BSA, 10% FBS in PBS for 30 min. Antibodies were prepared in 1% BSA/PBS and sections were stained overnight at 4°C. Secondary antibodies staining were performed for 1 hr at 4°C. Nuclei were stained with 10 uM DAPI for 10 min and slides were mounted with PBS/Glycerol. Antibodies are goat anti-GFP (Lifetechnologies),rabbit anti-RUNX2 (Novus) and rabbit anti-OSTERIX (Abcam). Fluorescent pictures were acquired with Leica DM5500B. Histological Staining of cartilage was performed after acquisition of the immunohistochemistry result using Alcian Blue 8GX for 25 min, rinsing in distilled water and counterstaining with 0.1% Nuclear fast red for 5 min. Overlapping regions were merged in ImageJ. Similarly, adipocytes were detected by washing with 60% isopropanol for 5 min, staining with Oil Red O (60% in Isopropanol) for 5 min and counter-staining with DAPI.

Gene expression profiling

All processing and analysis was performed with R bioconductor. Purified $CD45^-$ $Ter119^-$ $CD73^+$ $CD105^-$ and $CD45^-$ $Ter119^-$ $CD73^+$ $CD105^+$ cells were sorted in triplicate and RNA was hybridized on Affymetrix Mouse gene 1.0 ST array. Raw data was processed by Aroma and Limma package with RMA background correction and the quantile normalization method. The data is available at GEO. For cross-study comparisons, we used the following datasets: *Ebf2* GEO: GSE51608; *Cxcl12* GEO: GSE43613; *Nes* GEO: GSE21941; *Grem1* GEO: GSE57729; *Kitl* GEO: GSE33158; BSCP and lineages GEO: GSE64447. Raw CEL files were downloaded from GEO PubMed, processed by the R package Aroma and corrected for inter-studies effects by Combat in the SVA package in R. Replicates were merged into a representative profile by leaving out the least correlated one and averaging the remaining replicates. Hierarchical clustering was calculated based on Euclidean distance in R with the dendextend package. Gene annotations were based on Ensembl Biomart v82. Gene ontology enrichment was conducted with the topGO R package and genes differentially expressed with an adjusted p value below 0.05 were used for analysis with the Weight01 method using Kolmogorov-Smirnov statistics.

FACS

For BM stroma enrichment, biotin conjugated antibodies used for lineage depletion are Ter119 (Biolegend), CD31 (Mel, Biolegend), CD45 (30F11, Biolegend) and CD11b (M1/70, Biolegend). For HSC analysis, biotin conjugated antibodies for used lineage depletion are Ter119, CD31, CD11b, CD4 (RM4-5, Biolegend), CD8 (53-6.7, Biolegend), CD19 (6D5, Biolegend), and Gr-1 (RB6-8C5, Biolegend). For B cell analysis in the bone marrow, antibodies used are Gr1 (RB6-85C, Biolegend), CD3 (145-2C11, Biolegend), CD8a (53-6.7, Biolegend), CD43 (S7, BDbiosciences), IgM (RMM-1, Biolegend), IgD (11-26c.2a, Biolegend), BP-1 (6C3, Biolegend), CD24 (M1/69, Biolegend) and B220 (RA3-6B2, eBioscience). For B cells analysis in the spleen, antibodies used are Gr1 (RB6-85C, Biolegend), CD11b (M1/70, Biolegend), CD19 (eBio1D3, eBioscience), CD21 (eBio4E3, eBioscience), CD23 (B3B4, eBioscience), CD93 (AA4.1, Biolegend), B220 (RA3-6B2, eBioscience), IgM (RMM-1, Biolegend) and IgD (11-26c.2a, Biolegend). Other antibodies used are CD3 (17A2, Biolegend), B220 (RA3-6B2, eBioscience), CD34 (RAM34, Biolegend), CD44 (Pgp-1, Biolegend), CD48 (HM48-1, Biolegend), CD73 (Ty/11.8, Biolegend), CD105 (MJ7618, Ebioscience), CD140a (APA5, Biolegend), CD150 (TC15-12F122, Biolegend), CD117 (2B8, eBioScience), SCA1 (D7, Biolegend). TruStain FcX (Biolegend) was used to block Fc receptors. Streptavidin-Pacific Blue (Invitrogen) and Streptavidin-TexasRed (LifeTechnologies) were used as indirect labeling reagents for biotinylated antibodies. Dead cell exclusion was performed with DAPI. Flow cytometry was done on Cyan, LSR2 and FACS on BD FACS Aria II.

Light-sheet imaging of cleared bone samples

Mice were injected intraperitoneally with heparin (5 UI per g body weight) and intra-cardially perfused with PBS to remove blood. *Femurs were extracted and fixed in PFA 4% for 24 hr at 4°C. Samples were decalcified in 10% EDTA-PBS, changed twice per day,* for 4 days at 4°C. Femurs were then embedded in 5% low-melting agarose (Sigma) and the full BM cavity was exposed by vibratome-cutting (Leica VTS1200). Samples were blocked with TruStain FcX (Biolegend) in staining buffer (0.2% Gelatin,

2% Saponin, 0.02% Sodium Azide in PBS) for 2 days at 4°C. After washing in PBS, samples were incubated with biotin-conjugated CD4, CD8, CD11b, CD19, Ter119, Gr-1, CD48, CD41 (MWReg30, Biolegend) for the lineage cocktail (shown in cyan), PE-conjugated SCA1 (shown in white or red) and CD150-APC (shown in magenta; all Biolegend) in staining buffer for 2 days at 4°C. After washing in PBS, samples were incubated with Streptavidin-eFluor450 (Ebioscience) and 7-AAD (shown in blue; Sigma) for 1 day at 4°C. Samples were washed three times in PBS, 1 hr each and femurs were cleared according to SeeDB (Ke et al., 2013). After clearing, samples were mounted in agarose, placed in a chamber filled with clearing solution and imaged by a Z.1. Light-sheet microscope (Zeiss). Per sample, 50 image stacks with 600 slices each were obtained by tiled acquisition in 5 channels.

QUANTIFICATION AND STATISTICAL ANALYSIS

FCS files were first quality assessed in R with the FlowQ package and analyzed with the FlowCore package. Processing and data analysis of image stacks of the light-sheet microscopy analysis was performed in Fiji and Python. First, correction of chromatic offset was performed by calculating geometrical translation to align background intensities of orthogonal views in all channels. Then, nuclear spot detection was performed in the 7-AAD nuclear channel using a LoG Detector (Jaqaman et al., 2008). Spot centroids were used as seeds for segmentation in each channel using B-spline snakes for the slice at the centroid Z-position (Delgado-Gonzalo and Unser, 2013). The Snake-derived region of interest (sdROI) was used to calculate the median intensity if the area was between 20 and 150 μm^2 and the centroid of the sdROI is not more than 10 μm away from its associated nuclear spot. Otherwise a circular ROI of 50 μm^2 was used for intensity estimation. Registration was performed in Python with the Iterative Closest Point Algorithm of nuclear spots in adjacent views. Prior data analysis, outliers were removed by gating anatomic boundaries of the bone using Geographic Information System Shapely. Normalization of fluorescence across stacks was performed by standardizing mean fluorescence intensity (MFI) of each channel according to the MFI of nucleus intensity. For classification of cells, statistical analysis was performed for each set of markers by modeling intensities according to a Gaussian mixture distribution using SciKit (Pedregosa et al., 2011). Distances between HSC and stromal populations were computed using the k-nearest neighbors' algorithm (SciPy, Python, Jones et al., 2001). Density-based spatial clustering of HSC was performed with Dbscan, considering more than 4 cells per cluster within 40 μm (SciKit, Python). Statistical analysis of spatial point patterns was estimated with the inhomogeneous multitype pair correlation function with Ripley correction (Spatstats R package; Baddeley and Turner, 2005).

DATA AND SOFTWARE AVAILABILITY

The primary data of the gene expression profiling analysis reported in the paper have been submitted to GEO and are available under GEO: GSE79091. The corresponding code we generated for analysis is available here: https://github.com/jpabbuehl/SSC_microarrayAnalysis. The imaging data of bone marrow after HSC plus BMSC co-transplantation are available upon request. The code we generated to analyze this imaging data is available here: https://github.com/jpabbuehl/SSC_lightsheetAnalysis.